Journal Pre-proof

Auto- and paracrine rewiring of NIX-mediated mitophagy by insulin-like growth factor-binding protein 7 in septic AKI escalates inflammation-coupling tubular damage

Bang-Chuan Hu, Jing-Wen Zhu, Guo-Hua Wu, Juan-Juan Cai, Xue Yang, Zi-Qiang Shao, Yang Zheng, Jun-Mei Lai, Ye Shen, Xiang-Hong Yang, Jing-Quan Liu, Ren-Hua Sun, Hai-Ping Zhu, Xiang-Ming Ye, Shi-Jing Mo

PII: S0024-3205(23)00287-4

DOI: https://doi.org/10.1016/j.lfs.2023.121653

Reference: LFS 121653

To appear in: *Life Sciences*

Received date: 23 November 2022

Revised date: 13 March 2023

Accepted date: 26 March 2023

Please cite this article as: B.-C. Hu, J.-W. Zhu, G.-H. Wu, et al., Auto- and paracrine rewiring of NIX-mediated mitophagy by insulin-like growth factor-binding protein 7 in septic AKI escalates inflammation-coupling tubular damage, *Life Sciences* (2023), https://doi.org/10.1016/j.lfs.2023.121653

Auto- and paracrine rewiring of NIX-mediated mitophagy by insulin-like growth factor-binding protein 7 in septic AKI escalates inflammation-coupling tubular damage

Bang-Chuan Hu[1], Jing-Wen Zhu[1], Guo-Hua Wu[2], Juan-Juan Cai[3], Xue Yang[4], Zi-Qiang Shao[1], Yang Zheng[1], Jun-Mei Lai[5, 6], Ye Shen[5, 6], Xiang-Hong Yang[1], Jing-Quan Liu[1], Ren-Hua Sun[1], Hai-Ping Zhu[7], Xiang-Ming Ye[5, 6], Shi-Jing Mo[5, 6, 1*]

[1]*Emergency and Intensive Care Unit Center, Intensive Care Unit, Zhejiang Provincial People's Hospital, Affiliated People's Hospital, Hangzhou Medical College, Hangzhou 310014, Zhejiang, P.R.China*

[2]*Zhejiang University School of Medicine, Zhejiang University, Hangzhou 310029, Zhejiang, P.R.China*

[3]*Department of Pathology, Zhejiang Provincial People's Hospital, Affiliated People's Hospital, Hangzhou Medical College, Hangzhou 310014, Zhejiang, P.R.China*

[4]*Clinical Research Institute, Zhejiang Provincial People's Hospital, Affiliated People's Hospital, Hangzhou Medical College, Hangzhou 310014, Zhejiang, P.R.China*

[5]*Center for Rehabilitation Medicine, Department of Intensive Rehabilitation Care Unit, Zhejiang Provincial People's Hospital, Affiliated People's Hospital, Hangzhou Medical College, Hangzhou 310014, Zhejiang, P.R.China*

[6]*Center for Rehabilitation Medicine, Rehabilitation & Sports Medicine Research Institute of Zhejiang Province, Department of Rehabilitation Medicine, Zhejiang Provincial People's Hospital, Affiliated People's Hospital, Hangzhou Medical College, Hangzhou 310014, Zhejiang, P.R.China*

[7]*Department of Intensive Care Unit, The First Affiliated Hospital, Wenzhou Medical University, Wenzhou 325000, Zhejiang, P.R.China*

[*]**Corresponding author:**

Shi-Jing Mo, MD, PhD

Department of Intensive Rehabilitation Care Unit & Rehabilitation Medicine

Department of Intensive Care Unit

Zhejiang Provincial People's Hospital

Affiliated People's Hospital, Hangzhou Medical College

Hangzhou, Zhejiang 310014

P.R. China

Email: moshijing@hmc.edu.cn

ORCID: https://orcid.org/0000-0002-1303-4766

Abstract

Aims: Inflammation-coupling tubular damage (ICTD) contributes to pathogenesis of septic acute kidney injury (AKI), in which insulin-like growth factor-binding protein 7 (IGFBP-7) serves as a biomarker for risk stratification. The current study aims to discern how IGFBP-7 signalling influences ICTD, the mechanisms that underlie this process and whether blockade of the IGFBP-7-dependent ICTD might have therapeutic value for septic AKI.

Materials and Methods: In vivo characterization was carried out in B6/JGpt-*Igfbp7*^{em1Cd1165}/Gpt mice subjected to cecal ligation and puncture (CLP). Transmission electron microscopy, immunofluorescence, flow cytometry, immunoblotting, ELISA, RT-qPCR and dual-luciferase reporter assays were used to determine mitochondrial functions, cell apoptosis, cytokine secretion and gene transcription.

Key findings: ICTD augments the transcriptional activity and protein secretion of tubular IGFBP-7, which enables an auto- and paracrine signalling via deactivation of IGF-1 receptor (IGF-1R). Genetic knockout (KO) of *IGFBP-7* provides renal protection, improves survival and resolves inflammation in murine models of cecal ligation and puncture (CLP), while administering recombinant IGFBP-7 aggravates ICTD and inflammatory invasion. IGFBP-7 perpetuates ICTD in a NIX/BNIP3-indispensable fashion through dampening mitophagy that restricts redox robustness and preserves mitochondrial clearance programs. Adeno-associated viral vector 9 (AAV9)-NIX short hairpin RNA (shRNA) delivery ameliorates the anti-septic AKI phenotypes of *IGFBP-7* KO. Activation of BNIP3-mediated mitophagy by mitochonic acid-5 (MA-5) effectively attenuates the IGFBP-7-dependent ICTD and septic AKI in CLP mice.

Significance: Our findings identify IGFBP-7 is an auto- and paracrine manipulator of NIX-mediated mitophagy for ICTD escalation and propose that targeting the IGFBP-7-dependent ICTD represents a novel therapeutic strategy against septic AKI.

Key words: inflammation-coupling tubular damage, insulin-like growth factor-binding protein 7, mitophagy, septic acute kidney injury

1. Introduction

Acute kidney injury (AKI) initiated by sepsis is the leading cause of death among patients with severe and persistent infection in intensive care unit (ICU) and intensive rehabilitation care unit (IRCU). Despite recent advances in multimodality management [1, 2], therapeutic options for patients with septic AKI are limited and there is no satisfactory strategy in accelerating recovery. Generally, better understanding of pathophysiological mechanisms of septic AKI would be a principal paradigm shift in the potential treatment for this disorder.

Renal tubular epithelial cells (RTECs) simultaneously experience the lipopolysaccharide (LPS)-inducible inflammatory response and death-associated protein kinase 1 (DAPK1)-mediated apoptosis known as inflammation-coupling tubular damage (ICTD) during septic AKI, as reported in our previous study [3]. Occurrence of ICTD requires intracellular activation of DAPK1, the serine/threonine kinase that could be dephosphorylated at Ser308 under hypoxia for irreversible tubular apoptosis in a LPS-dependent manner. Like DAPK1, secreted protein peptide is also found to be a redox sensor associating with the LPS-inducible tubular apoptosis [4], indicating that driver of ICTD might not be always confined to the tubular cell-intrinsic molecules but can be extended to extracellular cytokines, especially the endocrine signalling.

Insulin-like growth factor-binding protein 7 (IGFBP-7) is a pleiotropic protein that modulates pathogenesis of diverse diseases including cancer, atherosclerosis, dyspnea and pulmonary arterial hypertension (PAH) [5-8]. IGFBP-7 is expressed ubiquitously and secreted by cells of various tissue types (e.g., fibroblasts, erythrocytes, vascular and epithelial cells). Earlier study demonstrate that IGFBP-7 deactivates IGF1 receptor (IGF1R) to trigger cell apoptosis [9]. IGFBP7 not only exerts direct anti-phagocytotic effects but also has a by-stander activity [10]. Although the functional role of IGFBP-7 remains poorly understood, the linkage between IGFBP-7 and prognosis or diagnosis of critically ill patients with AKI has been documented in several literature [11-13]. IGFBP-7 can also serve as a biomarker for risk stratification in septic AKI patients requiring renal replacement therapy [14]. Aberrant expression of IGFBP-7 has been associated with kidney dysfunction with diverse pathological settings, including cisplatin-, kidney ischemia/reperfusion- and lipopolysaccharide-induced AKI; IGFBP-7 inhibits tubular damage through blockade of poly [ADP-ribose] polymerase 1 (PARP1) degradation mediated by ring finger protein 4 (RNF4) [15]. However, the experimental significance of IGFBP-7 in

polymicrobial sepsis-elicited AKI has not been investigated, and little data on the reciprocity between IGFBP-7 and ICTD are available.

Here we establish that ICTD favors IGFBP-7 transcription and secretion, which in turn orchestrate an auto- and paracrine signalling through deactivation of IGF1R. Preclinical models demonstrate that genetic knockout (KO) of *IGFBP-7* allows cecal ligation and puncture (CLP) mice refractory to septic AKI and mortality, while administration of recombinant IGFBP-7 aggravates ICTD and inflammatory invasion. The auto- and paracrine IGFBP-7 signalling perpetuates ICTD mainly through restraining the NIX/BCL2/adenovirus E1B 19 kDa protein-interacting protein 3 (BNIP3)-mediated mitophagy. Kidney-specific deletion of NIX in CLP mice using adeno-associated viral vector serotype 9 (AAV9)-short hairpin RNA (shRNA) impairs the anti-septic AKI phenotypes of *IGFBP-7* KO. Activation of BNIP3-mediated mitophagy by mitochonic acid-5 (MA-5) prevents the IGFBP-7-dependent ICTD and septic AKI. Our findings offer new insights into the roles and mechanisms of auto- and paracrine IGFBP-7 signalling in ICTD and identify innovative strategy to increase the therapeutic repertoires against septic AKI.

2. Materials and Methods

2.1. Human subjects and serum IGFBP7 quantification

Serum samples of 27 patients who met the clinical criteria of septic AKI were collected from Intensive Care Unit (ICU) of Zhejiang Provincial People's Hospital for IGFBP-7 measurement. The exclusion criteria included: pregnancy, human immunodeficiency virus (HIV) infection, younger than 18 years, receiving radio-chemotherapy and inability to provide informed consent. Clinical information of these patients, including age, gender, Acute Physiology and Chronic Health Evaluation II [APACHE II] score, Sequential Organ Failure Assessment [SOFA] score and Kidney Disease Improving Global Outcomes [KDIGO] stage, were listed in Supplemental Table 1. A cohort of twenty-seven healthy donors in the medical examination center of Zhejiang Provincial People's Hospital were also recruited in this study with individual data: 17 males and 10 females, and 11 persons ≥ sixty years old and 16 persons < sixty years old. Study protocol concerning human subjects was approved by the Clinical Research Ethics Committee of Zhejiang Provincial People's Hospital, Hangzhou Medical College, study number 2020KY011. The study was conducted in accordance with the principles of the Declaration-of-Helsinki and written informed consent was obtained from all human subjects.

Serum IGFBP7 levels were measured by Human IGFBP-rp1/IGFBP-7 DuoSet ELISA Kit (R&D Systems Inc., cat#DY1334-05). The coefficient of variation was less than 10% and samples were diluted 20- to 100-fold to ensure that the enzymatic reaction was maintained within the linear range.

2.2. Reagents, constructs and antibodies

Recombinant mouse IGFBP-7 (IGFBP-7, cat#2120-B7-025) and human IGFBP-7 (rhIGFBP-7, cat#10163-B7-050) were ordered from R&D Systems (Minneapolis, MN). IGF1 (cat#sc-4590) was from Santa Cruz Biotechnology (Santa Cruz, CA). OSI-906 (cat#S1091) was from Selleck Chemicals LLC (Houston, TX). Liensinine (cat#HY-N0484), mitochonic acid-5 (cat#HY-111536), DAPK1 inhibitor (cat#HY-15847), zVAD-FMK (cat#HY-16658B) and necrostatin-1 (cat#HY-15760) were purchased from Medchem Express (Monmouth Junction, New Jersey, USA). Annexin V-FITC Apoptosis Detection Kit (cat#C1062L) was ordered from Beyotime (Nanjing, China). DAPK1 shRNA and siRNA duplexes targeting PINK1 and PARK2 were as previously described [3, 16].

Antibodies against COX IV (#SAB4503384), anti-PINK1 (#P0076) and anti-PARK2 (#SAB2500749) were ordered from Sigma-Aldrich (St.Louis, MO). Antibody against p-DAPK1_Ser308 (#PA5-105788) was from Thermo Fisher Scientific (San Diego, CA). Antibodies against IGF1Rβ (#9750), phospho-IGF1Rβ_Tyr1316 (#28897) and cleaved caspase-3 (#9661) were from Cell Signaling Technology (Danvers, MA). Antibodies against DAPK1 (#25136-1-AP) and HIF-1α (#66730-1-Ig) were obtained from Proteintech Group, Inc. (Chicago, IL). Antibodies against IGFBP-7 (#ab74169) was purchased from Abcam (Cambridge, MA, USA). Antibody against TOMM20 (#NBP1-81556) was from Novus Biologicals (Colorado, US, USA). IGFBP-7 neutralizing antibody (#MAB21201) was purchased from R&D Systems (Minneapolis, MN). Antibodies against NIX (#bs-5798R) and GAPDH (#bs-0755R) were from Biosynthesis (Beijing, China).

2.3. Animals and in vivo procedures

B6/JGpt-*Igfbp7*^{em1Cd1165}/Gpt mice (#T002861) were purchased from GemPharmatech Co. (Nanjing, China) and bred in the Laboratory Animal Center of Hangzhou Medical College in a specific-pathogen-free facility (Hangzhou, China). C57BL/6J littermates were served as the wild-type controls. *DAPK1*$^{-/-}$ mice were as previously described [3]. All animal experiments were conducted in accordance with the National Institutes of Health guide for the care and use of laboratory animals and were approved by the Ethics Committee on Use and Care of Animals of Hangzhou Medical College.

Murine models of cecal ligation and puncture (CLP) were performed as previously described [3, 16-18]. In brief, 2.0 cm of the cecum was mobilized and ligated with a 4-0 silk suture after midline laparotomy under ketamine (100 mg/kg) anesthesia. The mobilized cecum was then punctured with a 22-gauge needle and pressed to produce fecal material. Sham control animals underwent the same midline incision in abdomen followed by isolation of the cecum without ligation or puncture. All mice were received s.c. injection of imipenem/cilastatin (20 mg/kg) at the time of CLP. For therapeutic evaluation, 80 mg/kg mitochonic acid-5 (MA-5) was administered to CLP mice by oral gavage in combination with or without intravenous (i.v.) injection of recombinant mouse IGFBP-7 (1.5 mg/kg) per day until serum and kidneys were collected for analyses. Serum creatinine (Scr) was assessed using the Creatinine Enzymatic Reagent Set based on the provided protocol (Pointe Scientific, Canton, MI). BUN was measured using the QuantiChrom™ Urea Assay Kit (#DIUR-100) as directed by the manufacturer (BioAssay Systems, Hayward, CA). In interfering experiments, the shRNA cassette targeting mouse *NIX* was subcloned into adeno-associated virus 9 vector bearing the GFP-linked Ksp-cadherin promoter.

The oligonucleotides of AAV9-sh.NIX was: 5′-AGCTCGGCATCTATATT GGAAAGTGAAGCCACAGATGTTTCCAATATAGATGCCGAGCG-3′. After sequencing ensured accuracy of the vector, adeno-associated virus was packaged, purified and titrated by Vigene Biosciences (Shandong, China). Under anesthesia, mouse tail was swabbed with alcohol and injected intravenously with 100 μL of viral particles (1×10^{12} copies) harboring either the *NIX* or the control shRNA sequence. A correct injection was verified by noting blanching of the vein. After two weeks, renal tissues were harvested to evaluate the efficiency of delivery. The adeno-associated viruses were injected once per week. All mice were challenged with CLP as indicated or executed for further study.

To examine the effects of secreted IGFBP-7 in vivo, recombinant mouse IGFBP-7 (1.5 mg/kg, q.d) was administered to the *IGFBP-7*-V/T or -KO mice via tail vein injection for 2 days after CLP challenge. The indicated mice were sacrificed at 48 hours for sample collection and subsequent experiments.

2.4. Cell culture and transfections

Human kidney proximal tubular epithelial HK-2 cells derived from American Type Culture Collection (ATCC®, Manassas, Virginia, USA) were cultured in Dulbecco's modified Eagle's medium (Gibco, Carlsbad, USA) with 10% fetal bovine serum (FBS) as described previously [3, 16]. Renal tubular epithelial cells (RTECs) were isolated from renal cortices of the indicated mice using a procedure described in previous publications [16, 19] and grown in DMEM/F12 (Gibco) on collagen type 1-coated dishes at 37 °C in a humidified incubator containing 5% CO_2 and 95% air. For ICTD induction, cells were exposed to *Escherichia coli* 0111: B4 LPS under either physical hypoxia or 0.8 mmol/L Cobalt chloride ($CoCl_2$) preconditioning as previously reported [3].

For conditioned IGFBP-7 secretion in response to ICTD, RTECs (1×10^5) were seeded in 6-well plates and infected with lentiviral plasmids expressing RFP or RFP-IGFBP-7. The RFP- or RFP-IGFBP-7-expressed RTECs were next day transfected with IGFBP-7 sg.RNA and media was collected 48 h later, spin down to eliminate debris and used in subsequent experiments. Recipient RTECs were primed with LPS plus either physical hypoxia or Cobalt chloride ($CoCl_2$) for 8 h, after which they were treated with conditioned media (CM) as indicated in the presence or absence of recombinant mouse IGFBP-7 (25 ng/mL) addition. IGFBP-7 secretion was determined by enzyme-linked immunosorbent assay (ELISA) assays.

For experiments using blocking antibodies, RTECs seeded in 6-well dish were engineered to stably express RFP or RFP-IGFBP-7 and the secreted media was

harvested. Recipient RTECs were costimulated with LPS plus either physical hypoxia or Cobalt chloride ($CoCl_2$) for 8 h and then divided into four groups. One group was added with CM derived from RFP transfectants and 20 μg/mL anti-IgG antibody (R&D Systems, #AF007), another group was added with CM derived from RFP-IGFBP-7 transfectants and 20 μg/mL anti-IgG antibody. The third group was added with CM derived from RFP transfectants and 20 μg/mL IGFBP-7-specific neutralizing antibody, whereas the fourth group was added with CM derived from RFP-IGFBP-7 transfectants and 20 μg/mL IGFBP-7-specific neutralizing antibody. Recipient RTECs without LPS plus either physical hypoxia or Cobalt chloride ($CoCl_2$) costimuli in all groups served as control.

Small-interfering RNA (siRNA) transfection was performed as previously described [3, 16-18]. RTECs were cultured in 12-well plates and then transfected with 100 nmol/L small interfering RNA (siRNA) duplex oligonucleotides targeting NIX, PINK1 and PARK2, respectively, and corresponding control vectors that were constructed by the GenePharma company (Shanghai, China) using Lipofectamine™ RNAiMAX (Thermo Fisher Scientific) according to standard protocols. At 36 h post transfection, cells were harvested for further experiments.

2.5. Lentivirus packaging and CRISPR-Cas9 genome editing

Lentiviral plasmid coexpressing IGFBP7 and red fluorescent protein (RFP) was constructed by subcloning the full length mouse *IGFBP7* cDNA into pCDH-CMV-MCS-EF-1α-RFP-T2A+puro vector (#CD516B-2, System Biosciences, San Francisco, USA). Briefly, 293T cells were co-transfected with pCDH-CMV-MCS-EF-1α-RFP-T2A+puro-RFP-IGFBP-7, PMD29, PRRK and PRSV-REV in HEPES buffered saline (HBS) containing $CaCl_2$ (10 mmol/L). Viral supernatants were harvested 72 h later and passed through a 0.45 μm filter. Collected lentivirus was used to infect RTECs with addition of retronectin (Takara Bio Inc, Japan) and the transduced cells were selected with 1 μg/mL puromycin (Sigma Aldrich, St Louis, MO, USA).

For IGFBP-7 deletion by CRISPR-Cas9 technology, RTECs were cultured in DMEM media at a density of 1×10^4. Commercially available pCRISPR-LvSG03 lentiviral particles (Genecopoeia, Rockville, MD, #LPPMCP273701L03-1-200) were added based on formulas provided by user guide. Twenty-four hours later, the media containing lentiviral particles were removed and replaced with fresh medium. Next day, the transduced RTECs were cultivated with puromycin-added medium (working concentration 2 μg/mL) for selection. A small aliquot of cells was picked for deleting validation by western-blotting or real-time quantitative PCR (RT-qPCR).

2.6. Transmission electron microscopy

RTECs isolated from *IGFBP-7*-WT and -KO mice were exposed to 200 ng/mL recombinant mouse IGFBP-7 in the LPS-primed cultures under hypoxia for 12 h prior to fixation with 0.5 mol/L sodium cacodylate buffer (pH 7.4) containing 2% glutaraldehyde and formaldehyde at 4 °C. RTECs were then washed in 0.1 mol/L sodium cacodylate buffer, followed by secondary fixation with 1% osmium tetroxide and 1.5% potassium ferrocyanide at 20 °C. Two hours later, RTECs were washed by deionized water for five times and then incubated with 2% uranyl acetate in 0.1 mol/L maleate buffer (pH 5.5) before being embedded in Quetol epoxy resin. Images were taken on a Hitachi H7700 electron microscope. The mitochondrial fraction was calculated by computing the mean ratio of all single mitochondrial areas that fell within a cell using ImageJ software.

2.7. Reactive oxygen species (ROS) assay

For intracellular ROS detection, the indicated RTECs were incubated with 10 mmol/L DCFH-DA (Sigma-Aldrich, #D6883) at 37 °C for 30 min. Cells were then washed by PBS thrice and lysed with 50% methanol containing 0.1 M NaOH. After stripping and spinning at 4500 rpm for 5 min, the supernatants were transferred and fluorescence signal at 488/525 nm was detected by a Multimode Reader (Synergy H1, BioTek).

Mitochondrial reactive oxygen species (mtROS) were measured using MitoSOX^{TM} (Thermo Fisher Scientific, #M36008) as described in previous publication [16]. *IGFBP-7*-WT or -KO RTECs were stimulated with LPS under hypoxia for 8 h in the presence of 200 ng/mL recombinant mouse IGFBP-7 incubation and then loaded with 5 mmol/L MitoSOX for 30 min. After washing with PBS twice, fluorescence intensity was measured at 510/580 nm.

2.8. ATP, NAD$^+$/NADH, Δψm and cytosolic mtDNA measurement

RTECs grown in the LPS-supplemented medium under physical hypoxia in the presence or absence of 200 ng/mL recombinant mouse IGFBP-7 exposure were trypsinized and lysed to release ATP, the amounts of which were determined by ATP Detection Assay Kit (Cayman Chemical, #700410) according to the manufacturer's instructions.

NAD$^+$/NADH ratio was measured using NAD$^+$/NADH Cell-Based Assay kit (Cayman Chemical, #600480) according to the manufacturer's recommendation. In brief, RTECs bearing *NIX* siRNA were treated by CM as indicated under LPS plus physical hypoxia costimuli. Twelve hours later, RTECs were lysed and centrifuged.

Supernatants were then incubated in reaction solution for 1 h and absorbance was measured at 450 nm using FilterMax® plate reader.

Δψm was measured by TMRE Mitochondrial Membrane Potential Assay Kit (Biovision, #K238) as previously described [16]. Briefly, HK-2 cells costimulated with LPS plus physical hypoxia in the presence or absence of rhIGFBP-7 treatment were stained with 200 nmol/L TMRE for 30 min at room temperature. After washing with PBS, fluorescence intensity at 535/587 nm was determined by a FilterMax® plate reader.

Cytosolic mtDNA was analyzed as described previously [16]. In brief, DNA was purified from the cytosolic fractions of *IGFBP-7*-WT or -KO RTECs and mitochondrial DNA encoding cytochrome c oxidase 1 (COX1) was quantified by real-time quantitative PCR (RT-qPCR) with the following primer sequences:
Forward: 5′-GCCCCAGATATAGCATTCCC-3′
Reward: 5′-GTTCATCCTGTTCCTGCTCC-3′.
Nuclear DNA (evaluated by 18S ribosomal RNA) was used for normalization.

2.9. Mitochondrial isolation and western-blotting

Isolation of mitochondrial fractions from renal tissues and RTECs was performed using Mitochondria Isolation Kits (Thermo Fisher Scientific, #89801 and #89874) according to the manufacturer's guidelines, respectively. The mitochondria-enriched fractions were lysed in radioimmunoprecipitation assay (RIPA) buffer (Cwbiotech, Beijing, China) supplemented with phosphatase inhibitors and protease inhibitors and were sonicated for 3 minutes at 4 °C to shear contaminating genomic DNA before being loaded on sodium dodecyl sulfate (SDS)-polyacrylimide gel (PAGE).

Western-blotting was carried out on fractions from renal tissues and RTECs as previously described [16, 19-21]. In brief, lysates were centrifuged at 15, 000 g for 10 min at 4 °C and protein concentrations were determined using the Pierce BCA Assay (Thermo Scientific). Lysates were then mixed with 5× sample buffer containing 0.05% bromophenol blue, 0.5 mol/L dithiothreitol (DTT), 0.3 mol/L Tris-HCl (pH 6.8) and 50% glycerol for heat-denaturation at 95 °C, and fractionated on 10% SDS-PAGE electrophoresis, followed by transferring to the Immobilon™ PVDF Transfer Membranes (Millipore Corporation, Billerica, MA). Membranes were blocked for 45 min with 5% bovine serum albumin (BSA), probed with primary antibodies as indicated at 4 °C overnight and then incubated with the horseradish peroxidase (HRP)-conjugated secondary antibodies at room temperature. Signals were visualized by Western Chemiluminscent HRP Substrate Kit (PPLYGEN, Beijing, China).

2.10. Immunofluorescence

Procedures for immunocytochemistry (ICC) and immunohistofluorescence were as previously described [3, 16]. For ICC, the indicated RTECs were fixed with 4% paraformaldehyde in PBS for 30 min at 4 °C and blocked with 2% bovine serum albumin (BSA) in PBS. Incubation with the anti-cleaved Caspase-3 antibody (1:200) was carried out for 1 h at 20 °C, followed by incubation with secondary antibody conjugated to Alexa Fluor® 488 or 647 (Abcam) for 1 h at 20 °C. Images were captured on a fluorescent microscope (IX71; Olympus, Japan). To detect MitoTracker staining, RTECs were cultured overnight on glass coverslips, stained with 500 nmol/L MitoTracker™ Green (Thermo Fisher Scientific, #M7514) for 30 min at 37 °C, and washed twice with PBS. Cells were then fixed with 4% paraformaldehyde in PBS for 15 min and permeabilized with 0.2% Triton X-100. After blocking with 5% BSA, cells were incubated with primary antibodies overnight at 4 °C. Twenty-four hours later, RTECs were washed by PBS with Tween 20 (PBST) and incubated with secondary antibodies for 1 h at room temperature and then mounted with 4', 6-Diamidino-2-phenylindole (DAPI) in PBS for 15 min. For immunohistofluorescence, renal sections were permeabilized with 0.1% Triton X-100 for 15 min and blocked with 1% BSA and 0.1% Tween-20 in PBS for 1 hour at room temperature. Sections were then incubated with primary antibodies at 4 °C overnight. After extensive washing by 0.25% Triton X-100 in PBS, the Alexa Fluor® 647 secondary antibody was added to the blocking solution and incubated for 2 h. Sections were stained with DAPI and imaged on a Carl Zeiss (Oberkochen, Germany) Axioimager Z1 microscope.

2.11. Flow cytometry

Flow cytometry with Annexin V staining was carried out using Annexin V-FITC Apoptosis Detection Kit as previously described [18, 22]. In brief, the indicated RTECs were harvested, washed and resuspended in ice-cold binding buffer containing 25 μg/mL Annexin V-FITC. The mixture was incubated for 15 min at room temperature in the dark and then subjected to Fluorescence Activating Cell Sorter (FACS) analysis.

2.12. Cell viability assay

Cell viability was assessed by the 3-(4,5-dimethylthiazol-2-yl)-2,5-diphenyltetrazolium bromide reduction (MTT) assay as described in previous publications [18, 22]. Briefly, RTECs or HK-2 cells were seeded in 96-well plates at a density of 1×10^4 per well with the indicated treatment. Before the end of experiments,

20 μL MTT (5 mg/mL) was added and the plates were incubated at 37 °C for 4 h. Dimethyl sulfoxide was then added to dissolve formazan and the absorbance was measured at 570 nm by spectrometer (Wellscan MK3; Labsystems Dragon).

2.13. Enzyme-linked immunosorbent assay (ELISA)

IGFBP-7 concentrations of RTECs were determined by the colorimetric, sandwich-based RayBio® ELISA Kit (#Q61581, Shanghai, China) according to the manufacturer's instructions. HMGB1 (#ARG81310, Arigo), TNF (#ARG80206, Arigo), IL-17 (#M1700, R&D Systems) and IL-1β (#ARG80196, Arigo) were measured using commercially available enzyme-linked immunosorbent assay kits as indicated.

2.14. Real-time quantitative PCR (RT-qPCR)

RT-qPCR was performed according to previous protocols [3, 16-18]. In brief, the indicated kidney homogenates or RTECs were lysed and total RNA was extracted using RNeasy Plus Mini Kit (Qiagen, Hilden, Germany). Complementary DNA was synthesized using PrimeScript® RT Reagent Kit (Takana, Dalian, China) and real-time qPCR was carried out on an Applied Biosystems 7900HT cycler using Takana SYBR® Premix Ex Taq™ Kit (Takana) with the primers listed in Supplemental Table 2.

2.15. Dual-luciferase reporter (DLR) assay

DLR assay was carried out by a Dual-Luciferase Reporter Assay System Kit (Promega, Madison, WI) following the manufacturer's instructions as previously described [3, 18]. In brief, RTECs were seeded in 96-well plates for 24 h and then transfected with 100 ng of firefly luciferase reporter plasmids containing *IGFBP-7* gene promoter or non-promoter region and 1 ng of pRL-TK Renilla plasmids using Lipofectamine 3000 reagent (Invitrogen). Forty-eight hours later, the luciferase activities were measured by a Synergy 4 microplate reader (BioTek). The primers used for DLR in the current study were:

promoter (forward): 5′-CGAGCTACTGCTAAATATCCTAAAGAAAC-3′

promoter (reverse): 5′-CCCCGGGCAGAGAAGACCATTTAGAG-3′ .

non-promoter (forward): 5′-CGAGCTACCTCATCTGGAACAAGGTA-3′

non-promoter (reverse): 5′-CCCCGGGAGCGTCCTCCTTACTTAG-3′.

2.16. Gene Set Enrichment Analysis (GSEA)

For GSEA, gene expression dataset from GSE102453 were downloaded from Gene

Expression Omnibus (GEO) and incorporated into BROAD javaGSEA standalone version (http://www.broadinstitute.org/gsea/downloads.jsp) to examine the correlation of IGFBP-7 with mitophagy-related gene signature. The metric for ranking genes in GSEA was set as 'Pearson' and the other parameters were set to their default values.

2.17. Immunohistochemistry (IHC) and TdT-mediated dUTP nick end labelling (TUNEL) staining

IHC and TUNEL staining were conducted as described previously [3, 16, 18, 19]. Renal sections were fixed in 10% neutral buffered formalin and embedded in paraffin, followed by standard procedures with de-paraffinization and rehydratation. Antigen retrieval was performed in citrate buffer (pH 6.0) for 5 minutes in a pressure cooker. The endogenous peroxidase activity was quenched by incubation in 3% H_2O_2 in TBST for 15 min, followed by rinsing in water and blocking in 5% bovine serum albumin (BSA) in TBST. Immunohistochemical staining was performed using Dako ChemMateTM Envision^{TM} Detetcion Kit (DaKo, Glostrup, Denmark) after sections were probed with primary antibodies and incubated with horseradish peroxidase-conjugated secondary antibodies. Images were obtained with a AxioVision Rel.4.6 computerized image-analysis system (Carl Zeiss). TUNEL assay was performed with *In Situ* Cell Death Detection Kit from Roche Applied Science (Indianapolis, IN).

2.18. Statistical Analysis

Results were subjected to statistical analysis using SPSS 20.0 software (SPSS Inc, Chicago, IL, USA) and considered statistically significant if the P value was < 0.05. Survival curves were analyzed using the Kaplan-Meier method and P value was calculated by the log rank test. Two-tailed student's t-test has been used for comparisons of two groups. Two-sided ANOVA with Bonferroni procedure was applied for multiple comparisons.

3. Results

3.1. Auto- and paracrine IGFBP-7 signalling is boosted by ICTD during septic AKI

Our recent study demonstrated that renal tubular epithelial cells (RTECs) experience the LPS-inducible, DAPK1-mediated apoptosis known as ICTD in pathogenesis of septic acute kidney injury (AKI) [3]. To clarify the relationship between IGFBP-7/IGF1R axis and ICTD, we assessed the abundance of IGFBP-7 and IGF-1R in RTECs harvested from murine models of cecal ligation and puncture (CLP), which provides important insights into biological processes of polymicrobial sepsis [23]. We found that levels of IGFBP-7, but not IGF1R, were increased time-dependently after CLP challenge (Fig. 1A). To determine if the observed differences of IGFBP-7 abundance in RTECs could be recapitulated *in vivo*, we performed dichromatic immunofluorescence staining of IGFBP-7 and IGF1R in renal sections of CLP mice. Although IGF-1R$^+$ staining intensities were comparable in all sections tested, the proportion of IGFBP-7$^+$ staining was significantly higher in sections from CLP mice than in sections from control mice (Fig. 1B). These data implicate that IGFBP-7 signalling is boosted in tubular cells that experience ICTD during septic AKI.

We noticed that IGF-1R$^+$ immunostaining can be seen in both IGFBP-7$^+$ and adjacent IGFBP-7$^-$ cells. In fact, 16.5 ± 5.4% of cells in renal sections from CLP mice co-stained for IGFBP-7 and IGF-1R (Fig. 1B, right panel), raising the possibility that an auto- and paracrine IGFBP-7 signalling might occur in response to ICTD. To test this possibility, we enrolled a previously established cell model that mirrors ICTD *in vitro* [3]. In this configuration, RTECs were stimulated with LPS in the presence of either physical hypoxia or cobalt chloride ($CoCl_2$), and their *IGFBP-7* mRNA expression and promoter activity were then measured by real-time quantitative PCR (RT-qPCR) and dual-luciferase reporter (DLR) assays, respectively. LPS stimuli pronouncedly upregulated IGFBP-7 mRNA levels without alterations of IGF1R expression under hypoxic circumstances (Supplemental Fig. 1A), along with a higher *IGFBP-7* gene promoter activity (Supplemental Fig. 1B). Given transcriptional activation of *IGFBP-7* gene is required for protein secretion out of cells, we measured release of IGFBP-7 protein in the same inflammatory/hypoxic media using enzyme-linked immunosorbent assay (ELISA) and found that IGFBP-7 release of RTECs with LPS plus hypoxia costimuli was ∼2-fold higher than that of the parental cells without (Fig. 1C). These data together suggest that ICTD stimulates tubular IGFBP-7 secretion.

To directly interrogate the connection of auto- and paracrine IGFBP-7 signalling with ICTD, we exposed the LPS-stimulated RTECs to hypoxia, treated them with recombinant mouse IGFBP-7 protein (IGFBP-7) and then measured IGFBP-7 secretion. Treatment with IGFBP-7, which dose-dependently blocked the IGF1-inducible IGF-1R activation, increased IGFBP-7 release (Fig. 1D and Supplemental Fig. 1C), demonstrating that IGFBP-7 can induce its own secretion in response to ICTD. Deactivation of IGF-1R by OSI-906 also enhanced tubular IGFBP-7 secretion upon LPS plus hypoxia costimuli, but to a lesser degree than IGFBP-7 (Supplemental Fig. 1D). Given that pharmacological inhibitor may have off-target effects, we used a specific IGF-1R siRNA. Silencing IGF-1R in the LPS plus hypoxia-costimulated RTECs increased IGFBP-7 secretion as efficiently as OSI-906 did (Supplemental Fig. 1E). IGF1 tended to abrogate the LPS plus hypoxia-costimulated secretion of IGFBP-7 despite such abrogation did not reach statistical significance (Supplemental Fig. 1F). These results indicate that IGFBP-7 exerts an auto- and paracrine role on tubular cells, in which IGF-1R deactivation might be instrumental for the ICTD-stimulated secretion of its blocking ligand.

Activation of the auto- and paracrine IGFBP-7 signalling upon ICTD was further revealed by treating RTECs with condition medium (CM) derived from the red-fluorescent protein (RFP)-tagged IGFBP-7-transfected RTECs, which resulted in more IGFBP-7 secretion under the LPS plus hypoxia-costimulated circumstances in comparison to CM derived from the non-transfected or RFP-transfected RTECs (Fig. 1E-G). When ablating IGFBP-7 in the RFP-IGFBP-7-transfected RTECs with small guide RNA (sg.RNA) (Fig. 1G, right panel), their CM displayed less efficiency to increase IGFBP-7 secretion. However, this defect could be rescued by addition of IGFBP-7 (Fig. 1F). Thus, ICTD orchestrates an auto- and paracrine IGFBP-7 signalling that generates a positive feedback loop via IGFBP-7 secretion.

We next evaluated the relevance of our animal and cell findings to human pathology. To this end, we used serum from healthy donors or patients with septic AKI to treat human kidney proximal tubular epithelial HK-2 cells that were primed with LPS plus hypoxia (Fig. 1H and Supplemental Table 1). Septic AKI patient-derived serum had higher levels of IGFBP-7 and induced more IGFBP-7 secretion compared to the healthy donor-derived serum (Fig. 1I and Supplemental Fig. 1G). Thus, septic AKI patient-derived IGFBP-7 induces the ICTD-dependent IGFBP-7 secretion, which is equivalent to the effect as seen in RTECs.

To determine whether the serum IGFBP-7 is sufficient to orchestrate an auto- and paracrine signalling in kidney *in vivo*, we i.v. administered mice with recombinant mouse IGFBP-7 (1.5 mg/kg) once every day for consecutive five days. Compared to

vehicle, administration of IGFBP-7 markedly increased both blood and renal IGFBP-7 levels, reminiscent of CLP challenge (Supplemental Fig. 2A and 2B). Sera of these mice were then collected and intraperitoneal (i.p.) injected at dose of 200 μL into recipient mice, after which IGFBP-7 abundance in kidney samples was determined by RT-qPCR and enzyme-linked immunosorbent assay (ELISA), respectively. While the mRNA expression of IGFBP-7 in mice with sera injection did not differ significantly from those in mice without injection (Supplemental Fig. 2C), administering the IGFBP-7-replete sera led to higher IGFBP-7 secretion in kidney homogenate (Supplemental Fig. 2D), reinforcing the notion that systemic IGFBP-7 can orchestrate an auto- and paracrine signalling in kidney to promote secretion of itself.

3.2. Auto- and paracrine IGFBP-7 signalling aggravates ICTD and inflammatory invasion during septic AKI

The auto- and paracrine IGFBP-7 signalling boosted by ICTD during septic AKI prompted us to investigate its role in ICTD. For this purpose, the *IGFBP-7*-knockout (KO) mice and their wild-type (WT) littermates were subjected to CLP, followed by histopathological examination of renal sections using hematoxylin and eosin (H&E) staining, which showed that *IGFBP-7*-WT mice developed AKI after CLP challenge, characterized by tubulotoxic phenotypes including loss of epithelial brush border, tubular vacuolization and desquamation, whereas *IGFBP-7*-KO mice did these to a much lesser extent (Fig. 2A). In line with these findings, the percentage of cells positive for TdT-mediated dUTP nick end labelling (TUNEL) were reduced in renal sections of *IGFBP-7*-KO mice subjected to CLP (Fig. 2B). *IGFBP-7* KO made CLP mice refractory to mortality, yet there were no significant differences in survival duration between *IGFBP-7*-WT and -KO mice at healthy status (Fig. 2C). Upon CLP challenge, the levels of serum creatinine (Scr) and blood urea nitrogen (BUN) in *IGFBP-7*-KO mice were much lower than those in *IGFBP-7*-WT littermates (Fig. 2D). These data suggest that septic AKI could be alleviated in CLP mice lacking *IGFBP-7*.

To dissect whether IGFBP-7 deficiency modulates production of proinflammatory cytokines, we measured levels of interleukin-17 (IL-17), high mobility group box 1 (HMGB1), tumor necrosis factor (TNF) and interleukin-1β (IL-1β) in whole renal tissues of the *IGFBP-7*-KO and -WT mice subjected to CLP using enzyme-linked immunosorbent assay (ELISA). We observed that basal levels of the four proinflammatory cytokines in KO mice were comparable to those in WT mice, and their levels in WT mice were all elevated after CLP challenge. In contrast, only the production of HMGB1, but not that of IL-17, TNF and IL-1β, was profoundly

elevated in KO mice with CLP (Fig. 2E). Renal tissues of *IGFBP-7*-KO mice also had lower mRNA levels of *MCP-1*, *IL-6*, *KIM-1* and *BIM* than those of *IGFBP-7*-WT mice upon CLP challenge (Fig. 2F). These data suggest that IGFBP-7 deficiency constrains inflammatory invasion during septic AKI.

We then evaluated the role of secreted IGFBP-7 in septic AKI by administering intravenously (i.v.) recombinant mouse IGFBP-7 into CLP mice for two days. Administering IGFBP-7 led to worsened tubulotoxicity and apoptosis in renal sections of CLP mice (Fig. 3A and B). CLP mice receiving IGFBP-7 administration had higher levels of Scr and BUN than the control CLP mice, accompanied by the increased production of renal IL-17, TNF and IL-1β (Fig. 3C and D). To delineate whether the inhibitory effects of IGFBP-7 deficiency against septic AKI involve an IGFBP-7-dependent mechanism, we administered IGFBP-7 to the *IGFBP-7*-KO mice that were subjected to CLP. The worsened effects of IGFBP-7 on tubulotoxicity and apoptosis were abolished in KO mice (Fig. 3A and B).

To directly explore whether ICTD contributes to the exacerbated effects of IGFBP-7 in septic AKI, we employed immunohistochemistry (IHC) to detect DAPK1 Ser308 phosphorylation in renal sections of CLP mice receiving IGFBP-7 administration, which displayed reduced proportion of areas positive for staining as compared to those without administration (Fig. 3E). We also addressed whether ICTD influenced the extent of IGFBP-7 in septic AKI. In this setting, tubular damage was assessed by cleaved Caspase-3 (cCASP3) quantification using IHC. Administration of IGFBP-7 readily elevated cCASP3$^+$ staining intensity and such elevation was partially attenuated by DAPK1 inhibition (Fig. 3F). Thus, during septic AKI, the auto- and paracrine IGFBP-7 signalling perpetuates ICTD in which DAPK1 activation is a generalizable principle.

3.3. Auto- and paracrine IGFBP-7 signalling perpetuates ICTD in vitro

To verify the translation of auto- and paracrine IGFBP-7 signalling for aggravation of septic AKI to cell models, we examined the impact of IGFBP-7 on ICTD *in vitro*. IGFBP-7 increased death of RTECs with LPS plus either hypoxia or $CoCl_2$ costimuli, as reflected by flow cytometry (FCM) of Annexin-V staining analyses showing that the percentage of Annexin-V$^+$ dying cells was greatly increased following recombinant mouse IGFBP-7 exposure (Fig. 4A). Preincubation with the pan caspase inhibitor benzyloxycarbonyl-Val-Ala-Aspfluoromethylketone (zVAD-FMK), but not the necrosis inhibitor necrostatin-1, attenuated the IGFBP-7-increased cell death in the presence of LPS plus either hypoxia or $CoCl_2$ costimuli. These results indicate that IGFBP-7 perpetuates ICTD mediated by caspase activation.

To further characterize whether cell-derived IGFBP-7 perpetuates the caspase-mediated ICTD, we stimulated the RFP-IGFBP-7-transfected RTECs with LPS plus hypoxia or $CoCl_2$ and subjected these transfectants to immunocytochemistry (ICC) for apoptosis detection using cCASP3 staining (Supplemental Fig. 3A). A significantly larger number of cells underwent apoptosis after RFP-IGFBP-7 introduction. Of note, apoptosis not only occurred in the RFP-positive transfectants but also in neighboring cells that did not express RFP (Fig. 4B). To decipher whether secreted IGFBP-7 is functionally active, the LPS plus hypoxia- or $CoCl_2$-costimulated RTECs were treated with CM prepared from RFP-IGFBP-7 transfectants (Fig. 4C). As shown in Fig. 4D, CM from RFP-IGFBP-7 transfectants, but not that from RFP transfectants, increased apoptosis in RTECs with LPS plus hypoxia or $CoCl_2$ costimuli but not in those without. Nonetheless, neutralization of IGFBP-7 using a specific antibody (Ab) abrogated the apoptosis-inducible effect of CM from RFP-IGFBP-7 transfectants. The neutralizing IGFBP-7 Ab barely influenced survival of the LPS plus hypoxia- or $CoCl_2$-costimulated RTECs when incubating them with CM from RFP control transfectants. Thus, the auto- and paracrine IGFBP-7 signalling serves an important intermediate to perpetuate ICTD.

In concert with the aforementioned data that IGFBP-7 administration favors DAPK1 activation in renal sections of CLP mice, examination of DAPK1_Ser308 phosphorylation identified a prominent decrease in the LPS plus hypoxia- or $CoCl_2$-costimulated RTECs after IGFBP-7 exposure (Fig. 4E). Similar results were observed in human kidney proximal tubular epithelial HK-2 cells that were exposed to recombinant human IGFBP-7 (rhIGFBP-7) under the LPS-stimulated hypoxia circumstances (Supplemental Fig. 3B). However, IGFBP-7 increased death of DAPK1$^{-/-}$ RTECs to an equivalent degree as did in the DAPK1-intact RTECs (Supplemental Fig. 3C). The short hairpin RNA (shRNA)-mediated depletion of DAPK1 compromised death of HK-2 cells induced by LPS plus hypoxia, while it was unable to do so in the presence of rhIGFBP-7 exposure (Supplemental Fig. 3D). DAPK1$^{-/-}$ RTECs exhibited normal upregulation of *IGFBP-7* following LPS plus hypoxia costimuli (Supplemental Fig. 3E). These results implicate that the auto- and paracrine IGFBP-7 signalling perpetuates ICTD not mainly through activation of DAPK1.

To validate whether IGF1R deactivation is responsible for the observed ICTD perpetuation by IGFBP-7, we assessed cell viability of the LPS plus hypoxia-costimulated RTECs following IGF1 preincubation and found that RTECs with IGF1 preincubation had increased survival (Supplemental Fig. 3F). By contrary, OSI-906 treatment increased the LPS plus hypoxia-inducible cytotoxicity

(Supplemental Fig. 3G). Building on these observations, we exposed the IGF1R-silenced RTECs to IGFBP-7 to see if cytotoxicity could become less susceptible. Although silencing of IGF1R seems to abolish cell death following low-dose IGFBP-7 exposure, IGFBP-7 at higher concentration led to great cytotoxicity irrespective of IGF1R status upon LPS plus hypoxia costimuli (Supplemental Fig. 3H), suggesting that alternative mechanisms might be involved in the perpetuating role of auto- and paracrine IGFBP-7 signalling in ICTD.

3.4. NIX-mediated mitophagy compromises ICTD perpetuated by IGFBP-7

We next sought to surmise the predominant mechanism whereby IGFBP-7 perpetuates ICTD. The IGFBP-7-deficient RTECs experienced much less death in comparison to the IGFBP-7-proficient RTECs after being exposed to IGFBP-7 under the LPS-stimulated hypoxia conditions (Supplemental Fig. 4A and B), suggesting that intracellular IGFBP-7 is essential for the perpetuating role of auto- and paracrine IGFBP-7 signalling in ICTD. We thus decided to explore the role of endogenous IGFBP-7 in ICTD perpetuated by the auto- and paracrine IGFBP-7 signalling using RTECs from *IGFBP-7*-KO mice (Fig. 5A). We observed that *IGFBP-7*-KO RTECs were refractory to the IGFBP-7-inducible apoptosis upon LPS plus hypoxia costimuli (Supplemental Fig. 4C-E), which kinetically correlated with the declined levels of cytoplasmic and mitochondrial reactive oxygen species (ROS) (Fig. 5B) as judged by DCF-DA and MitoSOX fluorescent intensity, respectively. Alongside the diminished cytoplasmic and mitochondrial ROS, examination of RTECs from *IGFBP-7*-KO mice subjected to CLP using transmission electron microscopy (TEM) confirmed a great reduction in the mitochondrial fraction upon IGFBP-7 exposure (Fig. 5C and E). RTECs from *IGFBP-7*-KO mice with CLP also displayed significantly weaker MitoTracker Green staining than those from *IGFBP-7*-WT littermates with CLP in the presence of IGFBP-7 exposure (Fig. 5F), implying a diminution in mitochondrial mass.

Mitochondrial mass is determined by mitophagy, the evolutionarily conserved biological process through which cells selectively eradicate damaged mitochondria [24]. Mitophagy plays a principal role in mitochondrial homeostasis for tubular protection under stressful circumstances [25]. Consistent with its role in apoptosis inhibition, mitophagy is hallmarked by loss of mitochondrial membrane potential (ψm), reduction in mitochondrial reactive oxygen species (mtROS) and release of fragmented mtDNA to cytosol as well as elevation of intracellular adenosine triphosphate (ATP) [26, 27]. In mammalian cells, adenosine monophosphate-activated protein kinase (AMPK) provokes mitophagy via inducing phosphorylation of ULK1

at Ser555 [28]. Both PTEN-induced kinase 1 (PINK1) and parkin RBR E3 ubiquitin protein ligase (PARK2) have been previously shown to counteract septic AKI via mitophagy—the effect that could also recapitulate in the setting of persistent activation of NIX/BCL2 and adenovirus E1B 19-kDa-interacting protein 3 (BNIP3) pathway [29, 30]. Based on these hints and evidence, we investigated if mitophagy is involved in the IGFBP-7-perpetuated ICTD. To this end, RTECs were pretreated with the mitophagy inhibitor liensinine and then exposed to IGFBP-7 in the presence of LPS plus hypoxia costimuli. IGFBP-7 remarkably increased cytotoxicity of RTECs but could no longer to do so when these cells were pretreated with liensinine (Fig. 5G). Notably and in accordance with these results, blockade of mitophagy through small interfering RNA (siRNA)-directed silencing of NIX, but not that of PINK1 or PARK2, yielded comparable results (Fig. 5H and I), underscoring an inhibitory role of NIX-mediated mitophagy in the IGFBP-7-perpetuated ICTD.

Given NIX inhibits the IGFBP-7-perpetuated ICTD, we considered whether the NIX-mediated mitophagy was reprogrammed in this setting. Forced expression of IGFBP-7 in the LPS plus hypoxia-costimulated RTECs resulted in decreased mRNA expression of NIX but not that of PINK1 or PARK2 (Supplemental Fig. 4F). Vice versa, IGFBP-7 ablation increased NIX protein abundance in the mitochondrial fraction, while this effect could be abrogated by reconstituted expression of IGFBP-7 (Fig. 6A). The increased mitochondrial NIX was also detected in *IGFBP-7*-KO RTECs costimulated with LPS and hypoxia (Supplemental Fig. 4G), demonstrating an engagement of IGFBP-7 in controlling NIX levels in response to ICTD. In echoing this notion, we observed increased NIX mRNA expression in RTECs from *IGFBP-7*-KO mice in comparison to those from *IGFBP-7*-WT mice upon CLP challenge (Supplemental Fig. 4H), suggesting that the auto- and paracrine IGFBP-7 signalling represses NIX of tubular cells during septic AKI. To address how NIX expression varies in the progression of septic AKI, we examined NIX levels by IHC in renal sections of CLP mice. Relative to normal tubules, NIX staining in AKI lesions began to be detectable as early as 4 h following CLP challenge, peaked at 12 h and became implicit at 24 h and 48 h, respectively (Fig. 6B). In sharp contrast, levels of p-ULK1_Ser555 were not intensified until later timepoints, indicating that the NIX-mediated mitophagy might be an early event distinct from that mediated by AMPK-ULK1 axis during septic AKI. In parallel, the mitochondrial fractions of a series of renal samples derived from *IGFBP-7*-KO mice exhibited higher levels of mitochondrial NIX protein than those derived from *IGFBP-7*-WT mice upon CLP challenge (Fig. 6C).

3.5. IGFBP-7 rewires NIX-mediated mitophagy in response to ICTD

Next, we attempted to persue how IGFBP-7 regulates mitophagy during ICTD. In this effort, expression levels of translocase of outer mitochondrial membrane 20 homolog (TOMM20) protein in the LPS plus hypoxia-costimulated RTECs were analyzed after IGFBP-7 exposure. We observed that IGFBP-7 mitigated the LPS plus hypoxia-costimulated degradation of TOMM20 protein irrespective of NIX status but such mitigation could be further strengthened when PINK1 or PARK2 had been silenced (Fig. 6D and Supplemental Fig. 5A). Exposure of the LPS plus hypoxia-costimulated RTECs to IGFBP-7 robustly decreased intracellular ATP of these cells (Fig. 6E), which is likely explanation accounting for the observed ICTD perpetuation. Upon LPS and hypoxia costimuli, NAD^+/NADH ratio of the NIX-silenced RTECs treated with CM from RFP-IGFBP-7 transfectants was comparable to that of the silenced RTECs treating with CM from control RFP transfectants (Supplemental Fig. 5B). Together, these results corroborate that IGFBP-7 perpetuates ICTD via rewiring the NIX-mediated mitophagy.

We extended our investigation with respect to the rewiring role of IGFBP-7 in mitophagy by analyzing the LPS plus hypoxia-costimulated HK-2 cells, whose ψm magnitude was augmented after rhIGFBP-7 exposure (Fig. 6F). In RTECs with LPS plus hypoxia costimuli, *IGFBP-7* KO circumvented release of the fragmented mtDNA to cytosol (Fig. 6G and H). These observations were in agreement with the immunofluorescence analyses that ectopic expression of IGFBP-7 in the costimulated RTECs substantially blunted the capacity of LPS and hypoxia to increase light chain 3 (LC3) puncta (Fig. 6I-K). In renal sections of CLP mice, TOMM20 protein accumulation was disrupted—possibly as a compensatory mechanism for RTECs to adapt to the inflammatory/hypoxic stress and acquire the ability to overcome ICTD. *IGFBP-7* KO resulted in the most degradation of TOMM20 protein, whose levels had been normalized after IGFBP-7 administration (Supplemental Fig. 5C), coincide with our *in vitro* findings that the LPS plus hypoxia-costimulated degradation of TOMM20 protein became implicit following IGFBP-7 exposure. To interrogate whether IGFBP-7 rewires mitophagy in response to ICTD on a genetic background, we compared the transcriptional profile of *IGFBP-7*-KO and -WT RTECs with LPS plus hypoxia costimuli and found that mitophagy pathway genes were predominantly altered (Fig. 6L). Gene set enrichment analysis (GSEA) of a published expression profile [31] revealed that IGFBP-7 was inversely correlated with transcriptomics that reprogram the mitophagic signature around S1 tubules recently identified as antibacterial defense and the capacity to prevent CLP-related AKI in the setting of endotoxin preconditioning (Supplemental Fig. 5D). These results propose that the

auto- and paracrine IGFBP-7 signalling rewires mitophagy associated with ICTD.

3.6. Suppression of NIX-mediated mitophagy is instrumental for ICTD perpetuated by IGFBP-7 during septic AKI

Taken into account that silencing NIX renders resistance to ICTD perpetuated by IGFBP-7, we sought to discern whether the NIX-mediated mitophagy is responsible for septic AKI amelioration observed in *IGFBP-7*-KO mice. To approach this, we conditionally deleted NIX in the kidneys of *IGFBP-7*-KO mice via tail-vein injection of adeno-associated viral 9 (AAV9) harboring NIX shRNA (AAV9-sh.NIX) and randomized them to CLP procedure at 14 days after delivery. We confirmed that NIX was deleted throughout renal compartment with expression retained in other organs (i.e., lung or liver) (Fig. 7A-C). Mice with AAV9 harboring scrambled shRNA (AAV9-sh.Scr) delivery developed progressive AKI during the course of CLP experiments, unless *IGFBP-7* was knocked out, in case of which tubulotoxicity was deterred. Nevertheless, the AAV9-sh.NIX-delivered mice exhibited persistent tubulotoxicity even when *IGFBP-7* was knocked out (Fig. 7D and E). Compared with WT mice, tubular apoptosis was arrested in *IGFBP-7*-KO mice with AAV9-sh.Scr delivery upon CLP challenge, whereas such trend was not statistically significant in KO mice with AAV9-sh.NIX delivery (Fig. 7D and E). Accordingly, levels of Scr and BUN were declined in the AAV9-sh.Scr-delivered *IGFBP-7*-KO mice but tended to be rescued in the AAV9-sh.NIX-delivered KO mice upon CLP challenge (Fig. 7F). Renal samples of *IGFBP-7*-KO mice subjected to CLP had comparable levels of DAPK1 Ser308 phosphorylation regardless of NIX deletion (Supplemental Fig. 6A), suggesting that loss of NIX did not affect the inhibitory role of IGFBP-7 deficiency in DAPK1 activation.

Mitochonic acid 5 (MA-5), an indole derivative that modulates mitochondrial ATP synthesis and elicits mitophagy, efficiently prevents apoptosis via the BNIP3-mediated mitophagy [32, 33]. When CLP mice receiving IGFBP-7 administration possessed extensive AKI lesions and little disease-free tissues, CLP mice receiving MA-5 single treatment or MA-5 plus IGFBP-7 cotreatment retained a significantly larger fraction of normal renal tissues, demonstrating a delay in AKI development (Fig. 7G and H). Despite severe apoptosis was observed in renal sections of the IGFBP-7-administered CLP mice, renal sections of most MA-5 plus IGFBP-7-cotreated CLP mice displayed only mild apoptosis (Fig. 7G and H). Tubular protection conferred by MA-5 was associated with a drop of Scr and BUN levels in CLP mice with or without IGFBP-7 administration as well (Fig. 7I). Activation of the BNIP3-mediated mitophagy using MA-5 largely abolished the pro-apoptotic effects of

IGFBP-7 on the LPS plus hypoxia-costimulated RTECs (Supplemental Fig. 6B).

4. Discussion

ICTD is deemed to be a pivotal factor that governs septic AKI development. IGFBP-7 might become a potential therapeutic target for septic AKI as IGFBP-7 status has been linked to AKI prediction in patients with sepsis [34]. Mounting studies suggest that urinal IGFBP-7 serves as an independent diagnostic biomarker associated with AKI progression for critically ill patients [35-37]. Despite emerging insights for individual correlation of ICTD and IGFBP-7 with AKI, mechanisms underlying their interplay remain undefined and little actions to guide novel therapy are available. In the present study, we uncover a perpetuating role of the auto- and paracrine IGFBP-7 signalling in ICTD based on the following evidences: 1) IGFBP-7 and IGF1R colocalize in AKI lesions of CLP mice; 2) ICTD boosts IGFBP-7 transcription and secretion; 3) The ICTD-stimulated secretion of IGFBP-7 occurs in an IGFBP-7-dependent manner, which could be mediated by IGF1R deactivation; 4) Exogenous introduction of IGFBP-7 confers ICTD not only in IGFBP-7-positive but also in IGFBP-7-negative transfectants within the same culture; 5) Neutralization of IGFBP-7 perturbs the ability of conditioned medium (CM) from IGFBP-7 transfectants to perpetuate ICTD. It noteworthy that urinary IGFBP-7 excretion is increased in murine models of AKI [38]. TGF-β/Smad4 signalling pathway is responsible for transcription of *IGFBP-7*, and IGFBP-7 secretion contributes to the $BRAF^{V600E}$-mediated apoptosis [39, 40]. In this regard, IGFBP-7 could be viewed as an endocrine intermediate that links ICTD to septic AKI, and the possibility that septic AKI with increased IGFBP-7 secretion is more sensitive to TGF-β/Smad4 or $BRAF^{V600E}$ antagonists can not be ruled out. Our future work will aim to ascertain the precise molecular mechanism (s) of how ICTD modulates the auto- and paracrine IGFBP-7 signalling in tubules and dissect whether constitutive blockade of IGFBP-7 activity using small-molecule compound would be a feasible approach for septic AKI therapy.

Septic AKI is characterized by tubular damage as a result of systemic inflammatory response syndrome (SIRS) and cytokine storm. As the functional roles of the auto- and paracrine IGFBP-7 signalling in septic AKI could not fully be explained by the ICTD models *in vitro*, we used the *IGFBP-7*-KO mice. Consistent with the concept that secreted IGFBP-7 exaggerates inflammatory injury [41, 42], our data show that loss of IGFBP-7 attenuates tubular damage and prolongs survival duration of CLP mice. Intriguingly, renal production of IL-17, TNF and IL-1β, as well as mRNA expression of *MCP-1*, *IL-6*, *KIM-1* and *BIM*, in CLP mice were reduced after *IGFBP-7* KO. On the other hand, the histopathological analyses demonstrate

aggravated tubular damage in CLP mice receiving recombinant IGFBP-7 administration, which also boosts renal IL-17, TNF and IL-1β production as well as DAPK1 activation, suggesting that IGFBP-7 might sustain ICTD and inflammatory invasion during septic AKI.

The anti-septic effects of mitophagy have been studied like those of other types of autophagy. Studies from receptor-interacting serine/threonine-protein kinase 3 (RIPK3) and PINK1/PARK2 axis implicate that these pathways direct tubular mitophagy against septic AKI [16, 43, 44]. We present evidence here that the auto- and paracrine IGFBP-7 signalling can perpetuate ICTD by a previously unappreciated means: rewiring mitophagy mediated by NIX/BNIP3. We demonstrate that treatment with the mitophagy inhibitor liensinine or transfection with siRNA targeting NIX abrogates the IGFBP-7-perpetuated ICTD. IGFBP-7 loss can channel tubular cells away from oxidative stress and led to a shift towards decreased mitochondrial mass and an inhibition in apoptosis. IGFBP-7 abolishes mitochondrial NIX accumulation in response to ICTD, with a corresponding restoration in TOMM20 abundance, ATP expenditure and ψm magnitude—components of clearance program of defective mitochondria. Our results, together with studies reported previously, support the notion that termination of the NIX-mediated mitophagy plays a principal role in ICTD perpetuated by the auto- and paracrine IGFBP-7 signalling, which may be distinct from that initiated by the RIPK3- or PINK1/PARK2-dependent mitophagy responses.

Results from murine models of CLP suggest that deletion of renal NIX by AAV9-carrying shRNA delivery is generally considered to be effective in rescuing the anti-septic AKI phenotypes of *IGFBP-7* KO and spurs us to design further experiments to evaluate the efficacy of NIX/BNIP3 agonist in septic AKI. Our data reveal that MA-5 is preferentially to prevent the IGFBP-7-inducible ICTD *in vivo* and *in vitro*. We also propose that the anti-septic AKI efficacy of MA-5 would be tested in combination with apoptosis inhibitors, established agents as well as continuous renal replacement therapy (CRRT). Meanwhile, the optimal dose or therapeutic scheme of MA-5 still needed to be defined. This is particularly relevant when implementing combined studies with various treatments that are often managed over time.

There some limitations in our work. Although our study clearly demonstrate that IGFBP-7 contributes to the ICTD-inducible IGFBP-7 secretion via deactivation of IGF1R, this may not be the only mechanism because IGFBP-7 can also evoke other signalling routes [45]. So the auto- and paracrine IGFBP7 signalling with respect to septic AKI might be heterogeneous in cases of unknown IGFBP-7 receptors or additional signalling molecules. Beside mitophagy, the role of chaperone-mediated autophagy (CMA) in inflammatory diseases had also been studied due to the fact that

it shares similar properties with mitophagy [46, 47], so the intrinsic nature by which IGFBP-7 regulates CMA to perpetuate ICTD might be different. Herein, future studies are needed to test whether the auto- and paracrine IGFBP7 signalling perpetuates ICTD through rewiring CMA.

5. Conclusion

In summary, our study identifies a principal role of auto- and paracrine IGFBP-7 signalling in rewiring NIX-mediated mitophagy to perpetuate ICTD during septic AKI. ICTD favors transcription and secretion of tubular IGFBP-7 for induction of the auto- and paracrine signalling, which constrains the NIX-mediated mitophagy and thereby perpetuates ICTD and exacerbates septic AKI. Genetic loss of IGFBP-7 enables mice refractory to AKI and mortality launched by sepsis. Renal NIX deletion is sufficient to thwart the anti-septic AKI phenotypes caused by IGFBP-7 deficiency, whereas activation of NIX/BNIP3-mediated mitophagy prevents the IGFBP-7-perpetuated ICTD. Our data unearth the mechanisms whereby the auto- and paracrine IGFBP-7 signalling escalates ICTD and suggest that therapeutic targeting of the IGFBP-7-dependent ICTD might be a promising strategy for septic AKI management.

Funding

This work was supported by grants for National Natural Science Foundation of China (82102242 and 81971857); Natural Science Foundation of Zhejiang Province (LQ20H150009 and LQ20H150010), Zhejiang Provincial Traditional Chinese Medicine Science Research (2020ZB028) and Zhejiang Key R&D Project of Science Technology Department of Zhejiang Province (2019C03024).

CRediT authorship contribution statement

Bangchuan Hu: Investigation, Data curation, Formal analysis. Methodology, Writing – original draft, Funding acquisition. Jingwen Zhu, Guohua Wu, Juanjuan Cai and Xue Yang: Investigation, Formal analysis, Validation, Methodology. Ziqiang Shao, Yang Zheng, Junmei Lai and Ye Shen: Formal analysis, Methodology, Writing – review & editing. Xianghong Yang, Jingquan Liu, Renhua Sun, Haiping Zhu and Xiangming Ye: Resources, Writing – review & editing. Shijing Mo: Conceptualization, Supervision, Writing – original draft, Writing – review & editing, Project administration, Funding acquisition. All authors reviewed and approved the manuscript for publication.

Declaration of competing interest

The authors declare that there are no conflicts of interest.

Acknowledgments

We would show great gratitude for all participants.

References

[1] S. Peerapornratana, C.L. Manrique-Caballero, H. Gomez, J.A. Kellum, Acute kidney injury from sepsis: current concepts, epidemiology, pathophysiology, prevention and treatment, Kidney Int, 96 (2019) 1083-1099.

[2] R. Bellomo, J.A. Kellum, C. Ronco, R. Wald, J. Martensson, M. Maiden, S.M. Bagshaw, N.J. Glassford, Y. Lankadeva, S.T. Vaara, A. Schneider, Acute kidney injury in sepsis, Intensive Care Med, 43 (2017) 816-828.

[3] B.C. Hu, G.H. Wu, Z.Q. Shao, Y. Zheng, J.Q. Liu, R. Zhang, J. Hong, X.H. Yang, R.H. Sun, S.J. Mo, Redox DAPK1 destabilizes Pellino1 to govern inflammation-coupling tubular damage during septic AKI, Theranostics, 10 (2020) 11479-11496.

[4] Q.B. Lu, Q. Du, H.P. Wang, Z.H. Tang, Y.B. Wang, H.J. Sun, Salusin-beta mediates tubular cell apoptosis in acute kidney injury: Involvement of the PKC/ROS signaling pathway, Redox Biol, 30 (2020) 101411.

[5] M. Akiel, C. Guo, X. Li, D. Rajasekaran, R.G. Mendoza, C. Robertson, N. Jariwala, F. Yuan, M.A. Subler, J. Windle, D.K. Garcia, Z. Lai, H.H. Chen, Y. Chen, S. Giashuddin, P.B. Fisher, X.Y. Wang, D. Sarkar, IGFBP7 Deletion Promotes Hepatocellular Carcinoma, Cancer Res, 77 (2017) 4014-4025.

[6] A. Lisowska, P. Swiecki, M. Knapp, M. Gil, W.J. Musiał, K. Kaminski, T. Hirnle, A. Tycinska, Insulin-like growth factor-binding protein 7 (IGFBP 7) as a new biomarker in coronary heart disease, Adv Med Sci, 64 (2019) 195-201.

[7] N.E. Ibrahim, M. Afilalo, A. Chen-Tournoux, R.H. Christenson, H.K. Gaggin, J.E. Hollander, P. Kastner, P.D. Levy, A. Mang, S. Masson, J.T. Nagurney, R.M. Nowak, P.S. Pang, W.F. Peacock, V.R. Dipl-Stat, E.L. Walters, J.L. Januzzi, Jr., Diagnostic and Prognostic Utilities of Insulin-Like Growth Factor Binding Protein-7 in Patients With Dyspnea, JACC Heart Fail, 8 (2020) 415-422.

[8] H. Bouzina, R. Hesselstrand, G. Radegran, Plasma insulin-like growth factor binding protein 1 in pulmonary arterial hypertension, Scand Cardiovasc J, 55 (2021) 35-42.

[9] V. Evdokimova, C.E. Tognon, T. Benatar, W. Yang, K. Krutikov, M. Pollak, P.H. Sorensen, A. Seth, IGFBP7 binds to the IGF-1 receptor and blocks its activation by insulin-like growth factors, Sci Signal, 5 (2012) ra92.

[10] W.C. Lee, B. Russell, R.M. Sobota, K. Ghaffar, S.W. Howland, Z.X. Wong, A.G. Maier, D. Dorin-Semblat, S. Biswas, B. Gamain, Y.L. Lau, B. Malleret, C. Chu, F. Nosten, L. Renia, Plasmodium-infected erythrocytes induce secretion of IGFBP7 to form type II rosettes and escape phagocytosis, Elife, 9 (2020).

[11] F. Garnier, D. Daubin, R. Larcher, A.S. Bargnoux, L. Platon, V. Brunot, Y. Aarab, N. Besnard, A.M. Dupuy, B. Jung, J.P. Cristol, K. Klouche, Reversibility of Acute Kidney Injury in Medical ICU Patients: Predictability Performance of Urinary Tissue Inhibitor of Metalloproteinase-2 x Insulin-Like Growth Factor-Binding Protein 7 and Renal Resistive Index, Crit Care Med, 48 (2020) e277-e284.

[12] H.M. Jia, L.F. Huang, Y. Zheng, W.X. Li, Diagnostic value of urinary tissue inhibitor of metalloproteinase-2 and insulin-like growth factor binding protein 7 for acute kidney injury: a meta-analysis, Crit Care, 21 (2017) 77.

[13] A. Vijayan, S. Faubel, D.J. Askenazi, J. Cerda, W.H. Fissell, M. Heung, B.D. Humphreys, J.L. Koyner, K.D. Liu, G. Mour, T.D. Nolin, A. Bihorac, G. American Society of Nephrology Acute Kidney Injury

Advisory, Clinical Use of the Urine Biomarker [TIMP-2] x [IGFBP7] for Acute Kidney Injury Risk Assessment, Am J Kidney Dis, 68 (2016) 19-28.

[14] C. Nusshag, C. Rupp, F. Schmitt, E. Krautkramer, C. Speer, F. Kalble, S. Tamulyte, T. Bruckner, M. Zeier, J. Reiser, M.A. Weigand, F. Uhle, U. Merle, C. Morath, T. Brenner, Cell Cycle Biomarkers and Soluble Urokinase-Type Plasminogen Activator Receptor for the Prediction of Sepsis-Induced Acute Kidney Injury Requiring Renal Replacement Therapy: A Prospective, Exploratory Study, Crit Care Med, 47 (2019) e999-e1007.

[15] J.T. Yu, X.W. Hu, Q. Yang, R.R. Shan, Y. Zhang, Z.H. Dong, H.D. Li, J.N. Wang, C. Li, S.S. Xie, Y.H. Dong, W.J. Ni, L. Jiang, X.Q. Liu, B. Wei, J.G. Wen, M.M. Liu, Q. Chen, Y.R. Yang, G.Y. Zhang, H.M. Zang, J. Jin, Y.G. Wu, X. Zhong, J. Li, W. Wang, X.M. Meng, Insulin-like growth factor binding protein 7 promotes acute kidney injury by alleviating poly ADP ribose polymerase 1 degradation, Kidney Int, 102 (2022) 828-844.

[16] Z.D. Chen, B.C. Hu, X.P. Shao, J. Hong, Y. Zheng, R. Zhang, Z.Q. Shao, J.Q. Liu, X.H. Yang, R.H. Sun, S.J. Mo, Ascorbate uptake enables tubular mitophagy to prevent septic AKI by PINK1-PARK2 axis, Biochem Biophys Res Commun, 554 (2021) 158-165.

[17] J. Hong, B.C. Hu, L. Xu, Y. Zheng, Z.Q. Shao, R. Zhang, X.H. Yang, R.H. Sun, S.J. Mo, MicroRNA-19a Targets Fibroblast Growth Factor-Inducible Molecule 14 and Prevents Tubular Damage in Septic AKI, Anal Cell Pathol (Amst), 2020 (2020) 2894650.

[18] S.J. Mo, W. Zhang, J.Q. Liu, M.H. Chen, L. Xu, J. Hong, Q. Li, X.H. Yang, R.H. Sun, B.C. Hu, Regulation of Fn14 stability by SCF(Fbxw7alpha) during septic acute kidney injury, Am J Physiol Renal Physiol, 316 (2019) F1273-F1281.

[19] Y. Ni, B.C. Hu, G.H. Wu, Z.Q. Shao, Y. Zheng, R. Zhang, J. Jin, J. Hong, X.H. Yang, R.H. Sun, J.Q. Liu, S.J. Mo, Interruption of neutrophil extracellular traps formation dictates host defense and tubular HOXA5 stability to augment efficacy of anti-Fn14 therapy against septic AKI, Theranostics, 11 (2021) 9431-9451.

[20] L. Xu, Y. Jia, X.H. Yang, F. Han, Y. Zheng, Y. Ni, X. Chen, J. Hong, J.Q. Liu, Q. Li, R.H. Sun, S.J. Mo, MicroRNA-130b transcriptionally regulated by histone H3 deacetylation renders Akt ubiquitination and apoptosis resistance to 6-OHDA, Biochim Biophys Acta Mol Basis Dis, 1863 (2017) 1678-1689.

[21] Z.D. Chen, L. Xu, K.K. Tang, F.X. Gong, J.Q. Liu, Y. Ni, L.Z. Jiang, J. Hong, F. Han, Q. Li, X.H. Yang, R.H. Sun, S.J. Mo, NF-kappaB-dependent transcriptional upregulation of cyclin D1 exerts cytoprotection against hypoxic injury upon EGFR activation, Exp Cell Res, 347 (2016) 52-59.

[22] Y.K. Song, B.C. Hu, L. Xu, J.Q. Liu, X. Chen, Y. Zheng, M.H. Chen, J.Z. Wang, R.H. Sun, S.J. Mo, Productive transcription of miR-124-3p by RelA and RNA polymerase II directs RIP1 ubiquitination-dependent apoptosis resistance during hypoxia, Exp Cell Res, 378 (2019) 21-31.

[23] F.V. Sjaastad, I.J. Jensen, R.R. Berton, V.P. Badovinac, T.S. Griffith, Inducing Experimental Polymicrobial Sepsis by Cecal Ligation and Puncture, Curr Protoc Immunol, 131 (2020) e110.

[24] J. Zhu, K.Z. Wang, C.T. Chu, After the banquet: mitochondrial biogenesis, mitophagy, and cell survival, Autophagy, 9 (2013) 1663-1676.

[25] J. Sun, J. Zhang, J. Tian, G.M. Virzi, K. Digvijay, L. Cueto, Y. Yin, M.H. Rosner, C. Ronco, Mitochondria in Sepsis-Induced AKI, J Am Soc Nephrol, 30 (2019) 1151-1161.

[26] L. Montava-Garriga, I.G. Ganley, Outstanding Questions in Mitophagy: What We Do and Do Not Know, J Mol Biol, 432 (2020) 206-230.

[27] S.A. Killackey, D.J. Philpott, S.E. Girardin, Mitophagy pathways in health and disease, J Cell Biol, 219 (2020).

[28] D.F. Egan, D.B. Shackelford, M.M. Mihaylova, S. Gelino, R.A. Kohnz, W. Mair, D.S. Vasquez, A. Joshi, D.M. Gwinn, R. Taylor, J.M. Asara, J. Fitzpatrick, A. Dillin, B. Viollet, M. Kundu, M. Hansen, R.J. Shaw, Phosphorylation of ULK1 (hATG1) by AMP-activated protein kinase connects energy sensing to mitophagy, Science, 331 (2011) 456-461.

[29] C. Tang, H. Han, M. Yan, S. Zhu, J. Liu, Z. Liu, L. He, J. Tan, Y. Liu, H. Liu, L. Sun, S. Duan, Y. Peng, F. Liu, X.M. Yin, Z. Zhang, Z. Dong, PINK1-PRKN/PARK2 pathway of mitophagy is activated to protect against renal ischemia-reperfusion injury, Autophagy, 14 (2018) 880-897.

[30] Z.J. Fu, Z.Y. Wang, L. Xu, X.H. Chen, X.X. Li, W.T. Liao, H.K. Ma, M.D. Jiang, T.T. Xu, J. Xu, Y. Shen, B. Song, P.J. Gao, W.Q. Han, W. Zhang, HIF-1alpha-BNIP3-mediated mitophagy in tubular cells protects against renal ischemia/reperfusion injury, Redox Biol, 36 (2020) 101671.

[31] T. Hato, A. Zollman, Z. Plotkin, T.M. El-Achkar, B.F. Maier, S.L. Pay, S. Dube, P. Cabral, M. Yoshimoto, J. McClintick, P.C. Dagher, Endotoxin Preconditioning Reprograms S1 Tubules and Macrophages to Protect the Kidney, J Am Soc Nephrol, 29 (2018) 104-117.

[32] T. Suzuki, H. Yamaguchi, M. Kikusato, O. Hashizume, S. Nagatoishi, A. Matsuo, T. Sato, T. Kudo, T. Matsuhashi, K. Murayama, Y. Ohba, S. Watanabe, S. Kanno, D. Minaki, D. Saigusa, H. Shinbo, N. Mori, A. Yuri, M. Yokoro, E. Mishima, H. Shima, Y. Akiyama, Y. Takeuchi, K. Kikuchi, T. Toyohara, C. Suzuki, T. Ichimura, J. Anzai, M. Kohzuki, N. Mano, S. Kure, T. Yanagisawa, Y. Tomioka, M. Toyomizu, K. Tsumoto, K. Nakada, J.V. Bonventre, S. Ito, H. Osaka, K. Hayashi, T. Abe, Mitochonic Acid 5 Binds Mitochondria and Ameliorates Renal Tubular and Cardiac Myocyte Damage, J Am Soc Nephrol, 27 (2016) 1925-1932.

[33] Q. Lei, J. Tan, S. Yi, N. Wu, Y. Wang, H. Wu, Mitochonic acid 5 activates the MAPK-ERK-yap signaling pathways to protect mouse microglial BV-2 cells against TNFalpha-induced apoptosis via increased Bnip3-related mitophagy, Cell Mol Biol Lett, 23 (2018) 14.

[34] P.M. Honore, H.B. Nguyen, M. Gong, L.S. Chawla, S.M. Bagshaw, A. Artigas, J. Shi, O. Joannes-Boyau, J.L. Vincent, J.A. Kellum, Sapphire, I. Topaz, Urinary Tissue Inhibitor of Metalloproteinase-2 and Insulin-Like Growth Factor-Binding Protein 7 for Risk Stratification of Acute Kidney Injury in Patients With Sepsis, Crit Care Med, 44 (2016) 1851-1860.

[35] M. Fiorentino, Z. Xu, A. Smith, K. Singbartl, P.M. Palevsky, L.S. Chawla, D.T. Huang, D.M. Yealy, D.C. Angus, J.A. Kellum, ProCess, G. A.K.I. Pro, Serial Measurement of Cell-Cycle Arrest Biomarkers [TIMP-2] . [IGFBP7] and Risk for Progression to Death, Dialysis, or Severe Acute Kidney Injury in Patients with Septic Shock, Am J Respir Crit Care Med, 202 (2020) 1262-1270.

[36] I. Godi, S. De Rosa, F. Martino, S. Bazzano, M. Martin, E. Boni, M.R. Carta, C. Tamayo Diaz, G. Mari, A. Lorenzin, M. de Cal, V. Corradi, C. Caprara, D. Giavarina, C. Ronco, Urinary [TIMP-2] x [IGFBP7] and serum procalcitonin to predict and assess the risk for short-term outcomes in septic and non-septic critically ill patients, Ann Intensive Care, 10 (2020) 46.

[37] C. Adler, T. Heller, F. Schregel, H. Hagmann, M. Hellmich, J. Adler, H. Reuter, TIMP-2/IGFBP7 predicts acute kidney injury in out-of-hospital cardiac arrest survivors, Crit Care, 22 (2018) 126.

[38] A.C.M. Johnson, R.A. Zager, Mechanisms Underlying Increased TIMP2 and IGFBP7 Urinary Excretion in Experimental AKI, J Am Soc Nephrol, 29 (2018) 2157-2167.

[39] J. Watanabe, Y. Takiyama, J. Honjyo, Y. Makino, Y. Fujita, M. Tateno, M. Haneda, Role of IGFBP7 in Diabetic Nephropathy: TGF-beta1 Induces IGFBP7 via Smad2/4 in Human Renal Proximal Tubular Epithelial Cells, PLoS One, 11 (2016) e0150897.

[40] N. Wajapeyee, R.W. Serra, X. Zhu, M. Mahalingam, M.R. Green, Oncogenic BRAF induces senescence and apoptosis through pathways mediated by the secreted protein IGFBP7, Cell, 132 (2008) 363-374.

[41] Q. Yang, H.M. Zang, T. Xing, S.F. Zhang, C. Li, Y. Zhang, Y.H. Dong, X.W. Hu, J.T. Yu, J.G. Wen, J. Jin, J. Li, R. Zhao, T.T. Ma, X.M. Meng, Gypenoside XLIX protects against acute kidney injury by suppressing IGFBP7/IGF1R-mediated programmed cell death and inflammation, Phytomedicine, 85 (2021) 153541.

[42] Q. Xu, J. Wang, IGFBP7 aggravates sepsis-induced acute lung injury by activating the ERK1/2 pathway, Folia Histochem Cytobiol, 58 (2020) 247-254.

[43] A. Sureshbabu, E. Patino, K.C. Ma, K. Laursen, E.J. Finkelsztein, O. Akchurin, T. Muthukumar, S.W. Ryter, L. Gudas, A.M.K. Choi, M.E. Choi, RIPK3 promotes sepsis-induced acute kidney injury via mitochondrial dysfunction, JCI Insight, 3 (2018).

[44] Y. Wang, J. Zhu, Z. Liu, S. Shu, Y. Fu, Y. Liu, J. Cai, C. Tang, Y. Liu, X. Yin, Z. Dong, The PINK1/PARK2/optineurin pathway of mitophagy is activated for protection in septic acute kidney injury, Redox Biol, 38 (2021) 101767.

[45] R.J. Ferry, Jr., L.E. Katz, A. Grimberg, P. Cohen, S.A. Weinzimer, Cellular actions of insulin-like growth factor binding proteins, Horm Metab Res, 31 (1999) 192-202.

[46] Y. Hosaka, J. Araya, Y. Fujita, T. Kadota, K. Tsubouchi, M. Yoshida, S. Minagawa, H. Hara, H. Kawamoto, N. Watanabe, A. Ito, A. Ichikawa, N. Saito, K. Okuda, J. Watanabe, D. Takekoshi, H. Utsumi, M. Hashimoto, H. Wakui, S. Ito, T. Numata, S. Mori, H. Matsudaira, K. Hirano, T. Ohtsuka, K. Nakayama, K. Kuwano, Chaperone-Mediated Autophagy Suppresses Apoptosis via Regulation of the Unfolded Protein Response during Chronic Obstructive Pulmonary Disease Pathogenesis, J Immunol, 205 (2020) 1256-1267.

[47] W. Xie, L. Zhang, H. Jiao, L. Guan, J. Zha, X. Li, M. Wu, Z. Wang, J. Han, H. You, Chaperone-mediated autophagy prevents apoptosis by degrading BBC3/PUMA, Autophagy, 11 (2015) 1623-1635.

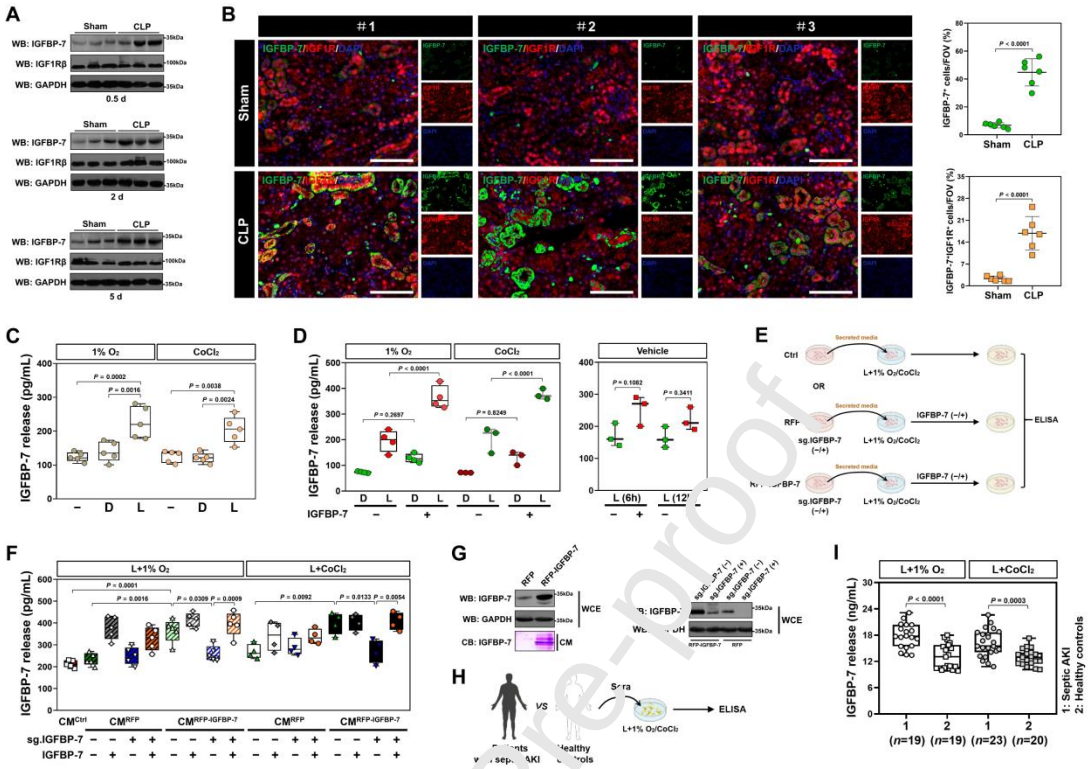

Fig. 1. Auto- and paracrine IGFBP-7 signalling is boosted by ICTD during septic AKI. A: Western-blotting analyses detecting levels of IGFBP-7 and IGF1Rβ protein in RTECs from sham and CLP mice at the indicated times (n = 3 per group). B: Representative immunofluorescence images and quantification of IGFBP-7$^+$ or IGFBP-7$^+$/IGF1R$^+$ staining in renal section from sham and CLP mice (n = 6 per group). Scale bar = 100 um. C: ELISA assay of IGFBP-7 secretion in RTECs cultures exposed to 150 ng/mL LPS under either physical hypoxia or 0.8 mmol/L Cobalt chloride ($CoCl_2$) preconditioning for 8 h (n = 5 per group). D, DMSO. L, LPS. D: ELISA assay of IGFBP-7 secretion in RTECs cultures exposed to 150 ng/mL LPS under either physical hypoxia or 0.8 mmol/L Cobalt chloride ($CoCl_2$) preconditioning in the presence or absence of recombinant mouse IGFBP-7 (IGFBP-7, 25 ng/mL) treatment ($n \geq 3$ per group). E: Experimental scheme of RTECs treated with conditioned medium (CM) from the indicated RTECs after being primed with LPS and hypoxia. F: ELISA assay of IGFBP-7 secretion in RTECs cultures in the presence of the indicated conditioned medium (CM) treatment with or without IGFBP-7 incubation after being primed with 150 ng/mL LPS under either physical hypoxia or 0.8 mmol/L Cobalt chloride ($CoCl_2$) preconditioning ($n \geq 4$ per group). Ctrl, control. sg.IGFBP-7, IGFBP-7 sgRNA. G: *Left panel:* western-blotting (WB) and coomassie blue (CB) analyses detecting levels of IGFBP-7 protein in whole cell extraction

(WCE) or conditioned medium (CM) of RFP-tagged IGFBP-7-expressed RTECs. *Right panel:* western-blotting (WB) analyses comparing levels of IGFBP-7 sgRNA (sg.IGFBP-7)-transfected RTECs where IGFBP-7 was deleted from the genome by CRISPR-Cas9 editing in the presence of RFP or RFP-IGFBP-7 overexpression. H: Schematic showing IGFBP-7 measurement in HK-2 cells with serum from patients with septic AKI and healthy volunteers upon LPS plus hypoxia costimuli. I: ELISA assay of IGFBP-7 secretion in HK-2 cells exposed to 150 ng/mL LPS under either physical hypoxia or 0.8 mmol/L Cobalt chloride ($CoCl_2$) preconditioning in the presence of sera from patients with septic AKI and healthy volunteers. Data are expressed as mean ± s.d. (B, C, D, F, I). Two-sided Student's *t* test (B) and two-sided ANOVA with Bonferroni post hoc *t* test correction (C, D, F, I) was used to calculate the *P* value, respectively.

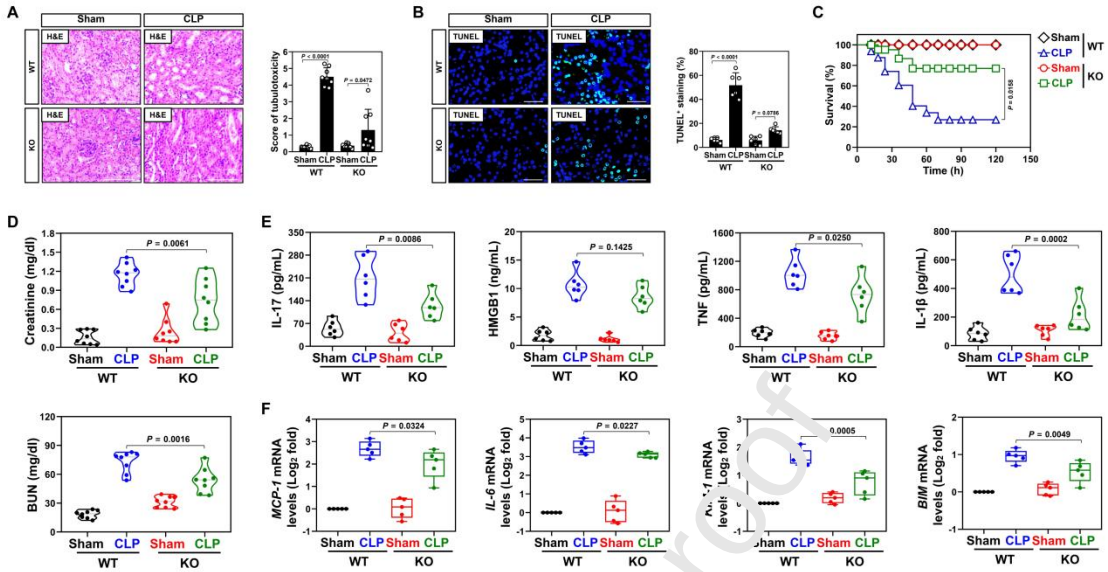

Fig. 2. Genetic disruption of *IGFBP-7* alleviates septic AKI. A: Representative hematoxylin and eosin (H&E) images and quantification of renal sections from *IGFBP-7*-WT or -KO mice with or without CLP challenge (n = 8 per group). Scale bar = 100 μm. B: Representative TUNEL images and quantification of renal sections from *IGFBP-7*-WT or -KO mice with or without CLP challenge (n = 6 per group). Scale bar = 50 μm. C: Kaplan-Meier curves analyzing the survival of *IGFBP-7*-WT or -KO mice with or without CLP challenge at the indicated times ($n \geq 10$ mice per group). D: Serum creatinine (Scr) and blood urea nitrogen (BUN) of *IGFBP-7*-WT or -KO mice with or without CLP challenge (n = 8 per group). E: ELISA assays measuring interleukin-17 (IL-17), high mobility group box 1 (HMGB1), tumor necrosis factor (TNF) and interleukin-1β (IL-1β) production in kidney homogenate of *IGFBP-7*-WT or -KO mice with or without CLP challenge (n = 6 per group). F: RT-qPCR analysis comparing mRNA levels of *monocyte chemoattractant protein-1* (*MCP-1*), *interleukin-6 (IL-6)*, *kidney injury molecule-1* (*KIM-1*) and *BIM* in kidney homogenate of *IGFBP-7*-WT or -KO mice with or without CLP challenge (n = 5 per group). Data are expressed as mean ± s.d. (A, B, D, E, F). Log-rank t test (C) and two-sided ANOVA with Bonferroni post hoc t test correction (A, B, D, E, F) was used to calculate the P value, respectively.

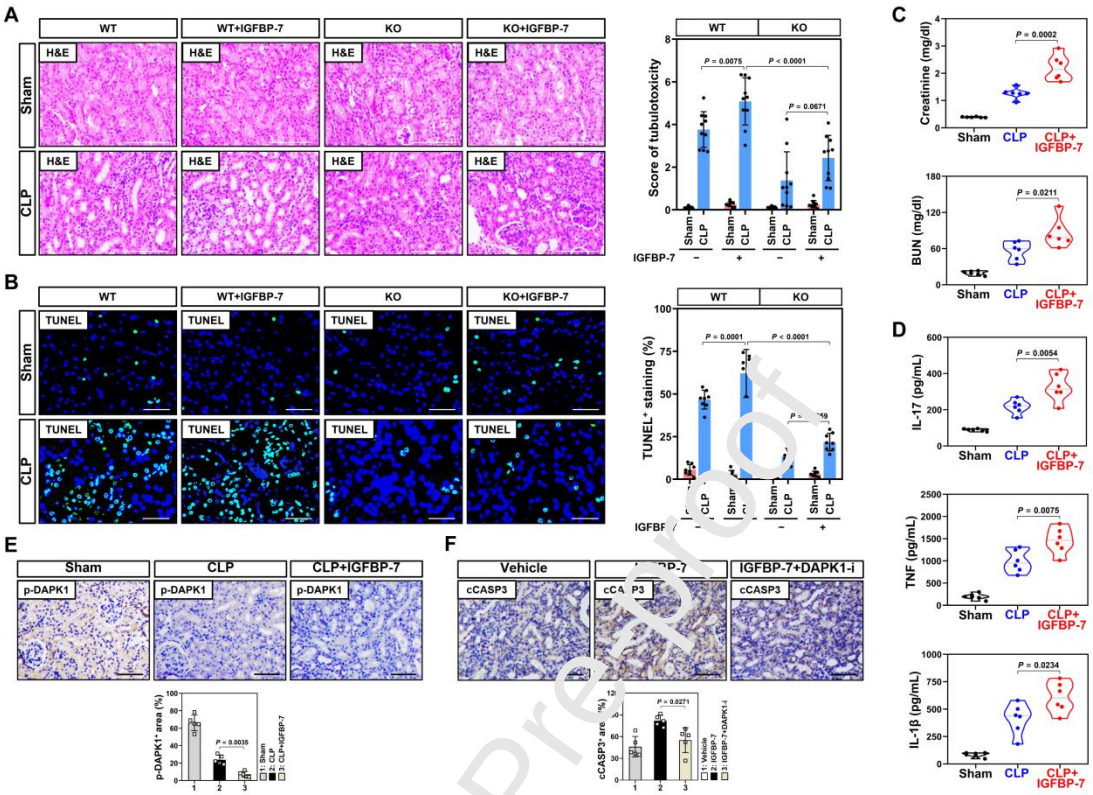

Fig. 3. IGFBP-7 aggravates ICTD and inflammatory invasion during septic AKI. A: Representative hematoxylin and eosin (H&E) images and quantification of renal sections from *IGFBP-7*-WT or -KO mice receiving injections of recombinant mouse IGFBP-7 (1.5 mg/kg) for 2 days after CLP challenge (n = 10 per group). Scale bar = 100 μm. B: Representative TUNEL images and quantification of renal sections from *IGFBP-7*-WT or -KO mice receiving injections of recombinant mouse IGFBP-7 (1.5 mg/kg) for 2 days after CLP challenge (n = 8 per group). Scale bar = 50 μm. C: Serum creatinine (Scr) and blood urea nitrogen (BUN) of CLP mice with or without injection of recombinant mouse IGFBP-7 (n = 6 per group). D: ELISA assays comparing interleukin-17 (IL-17), tumor necrosis factor (TNF) and interleukin-1β (IL-1β) production in kidney homogenate of CLP mice with or without injection of recombinant mouse IGFBP-7 (n = 6 per group). E: Representative IHC images for p-DAPK1_Ser308 staining of renal sections from CLP mice with or without injection of recombinant mouse IGFBP-7 (n = 5 per group). F: Representative IHC images for cleaved Caspase-3 (cCASP3) staining of renal sections from CLP mice receiving IGFBP-7 administration in the presence or absence of intraperitoneal (i.p.) injection of DAPK1 inhibitor (1 mg/kg) (n = 5 per group). Data are expressed as mean ± s.d. (A-F). Two-sided ANOVA with Bonferroni post hoc t test correction (A-F) was used

to calculate the *P* value.

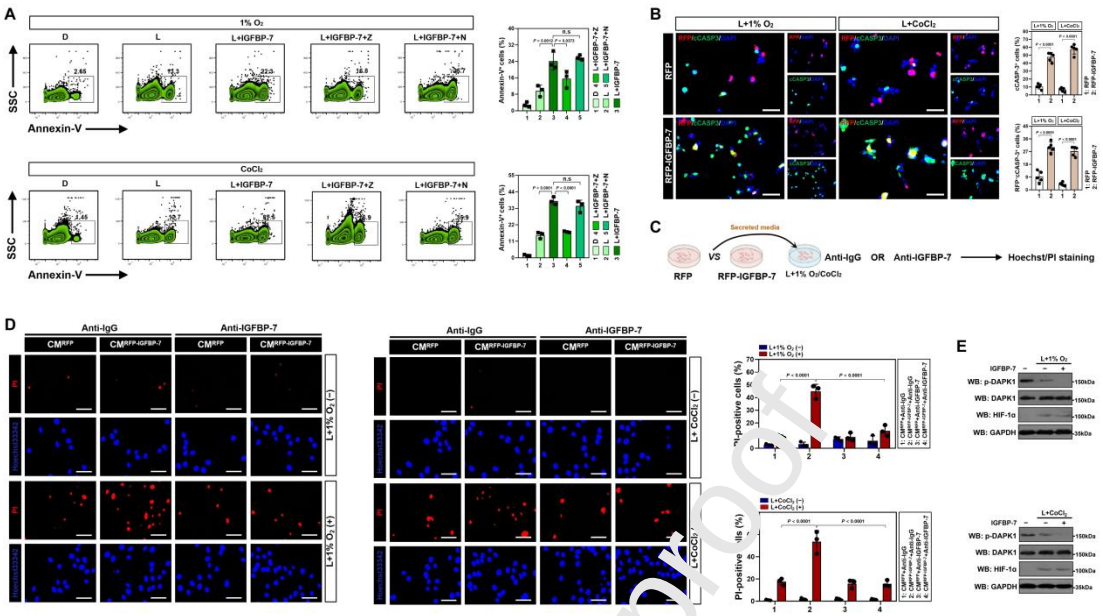

Fig. 4. Auto- and paracrine IGFBP-7 signalling perpetuates ICTD *in vitro*. A: Zebra plots and quantification of flow cytometry with Annexin-V staining in RTECs exposed to LPS stimuli or LPS plus IGFBP-7 (200 ng/mL) costimuli in the presence or absence of 20 μmol/L zVAD-FMK (Z) and 10 μmol/L Necrostatin-1 (N) under either physical hypoxia or 0.8 mmol/L Cobalt chloride ($CoCl_2$) preconditioning (*n* = 3 per group). D, DMSO. L, LPS. B: Representative immunfluorescence images and quantification of cleaved caspase-3$^+$ (cCASP3$^+$) or RFP$^-$/cCASP3$^+$ staining in RFP-tagged IGFBP-7-expressed RTECs exposed to LPS stimuli under physical hypoxia or 0.8 mmol/L Cobalt chloride ($CoCl_2$) preconditioning (*n* = 5 per group). Scale bar = 100 μm. C: Experimental scheme of the LPS plus physical hypoxia- or Cobalt chloride ($CoCl_2$)-costimulated RTECs with conditioned medium (CM) treatment from the RFP-tagged IGFBP-7-expressed RTECs in the presence of IGFBP-7 neutralizing antibody administration for Hoechst 33342 and PI double-staining assay. D: Representative images and quantification of Hoechst 33342 and PI double-staining in the LPS plus hypoxia-costimulated RTECs with conditioned medium (CM) treatment from the RFP-tagged IGFBP-7-expressed RTECs in the presence or absence of IGFBP-7 neutralizing antibody (20 μg/mL) incubation (*n* = 3 per group). Scale bar = 50 μm. E: Western-blotting (WB) analyses determining amount of DAPK1_Ser308 phosphorylation in RTECs with LPS plus hypoxia or 0.8 mmol/L Cobalt chloride ($CoCl_2$) costimuli in the presence or absence of IGFBP-7 treatment. Data are expressed as mean ± s.d. (A, B, D). Two-sided Student's *t* test (B) and two-sided ANOVA with Bonferroni post hoc *t* test correction (A, D) was used to

calculate the *P* value, respectively.

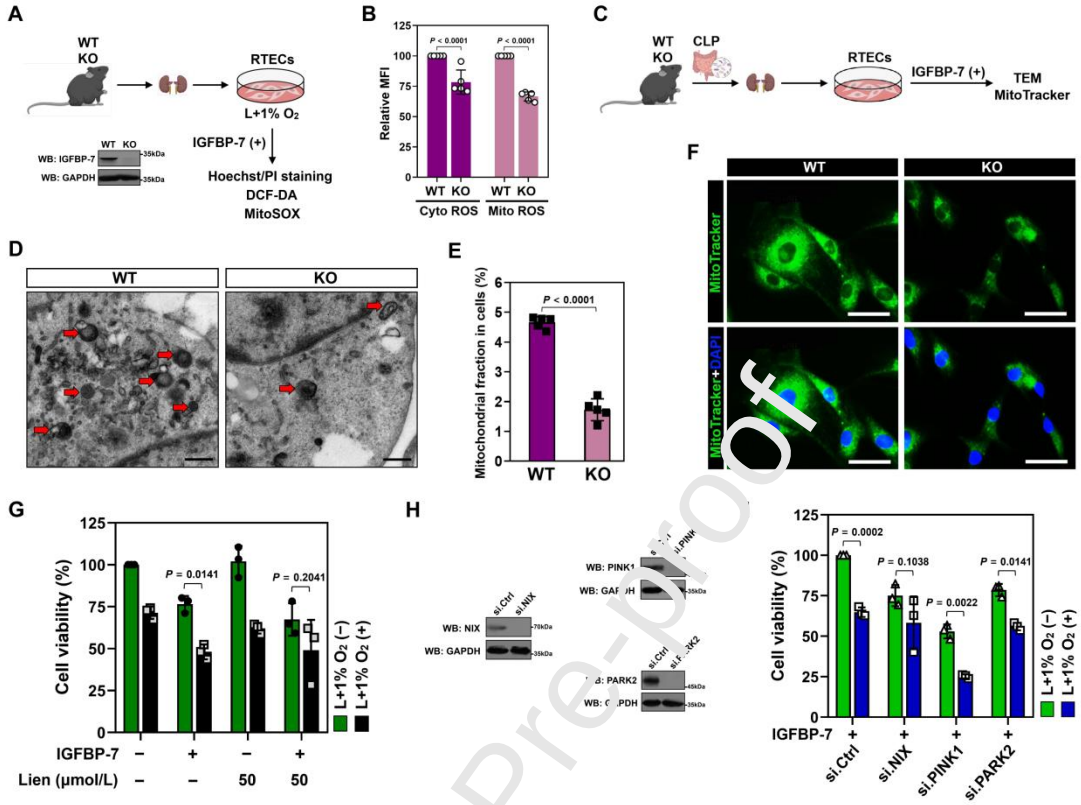

Fig. 5. IGFBP-7 perpetuates ICFD in a NIX-dependent manner. A: *Top panel:* experimental scheme of the LPS plus hypoxia-costimulated RTECs from *IGFBP-7*-WT or -KO mice for cytoplasmic and mitochondrial reactive oxygen species (ROS) detection by DCF-DA and MitoSOX staining upon IGFBP-7 exposure. *Bottom panel:* western-blotting (WB) analyses examining levels of IGFBP-7 protein in *IGFBP-7*-WT or -KO RTECs. B: Median fluorescent intensity (MFI) of cytoplasmic and mitochondrial ROS in *IGFBP-7*-WT or -KO RTECs with LPS plus hypoxia costimuli upon IGFBP-7 exposure (*n* = 5 per group). C: Experimental scheme of RTECs from *IGFBP-7*-WT or -KO mice with CLP challenge for transmission electron microscopy (TEM) analyses and MitoTracker Green staining in the presence of IGFBP-7. D and E: Representative images (D) and quantification (E) of transmission electron microscopy (TEM) examining mitochondrial fraction of RTECs from *IGFBP-7*-WT or -KO mice with CLP challenge in the presence of IGFBP-7 exposure (*n* = 5 per group). Scale bar = 0.5 μm. F: Representative MitoTracker Green images of RTECs from *IGFBP-7*-WT or -KO mice with CLP challenge in the presence of IGFBP-7 exposure. Scale bar = 25 μm. G: MTT assay detecting cell viability of the LPS plus hypoxia-costimulated RTECs with or without IGFBP-7 exposure in the presence or absence of 50 μmol/L liensinine (Lien)

treatment (*n* = 3 per group). H: Western-blotting (WB) analyses evaluating levels of NIX, PINK1 and PARK2 protein in RTECs transfected with siRNA targeting NIX (si.NIX), PINK1 (si.PINK1) or PARK2 (si.PARK2). Si.Ctrl, control siRNA. I: MTT assay detecting cell viability of the LPS plus hypoxia-costimulated RTECs with IGFBP-7 exposure in the presence or absence of siRNA targeting NIX (si.NIX), PINK1 (si.PINK1) or PARK2 (si.PARK2) transfection (*n* = 3 per group). Data are expressed as mean ± s.d. (B, E, G, I). Two-sided Student's *t* test (B, E) and two-sided ANOVA with Bonferroni post hoc *t* test correction (G, I) was used to calculate the *P* value, respectively.

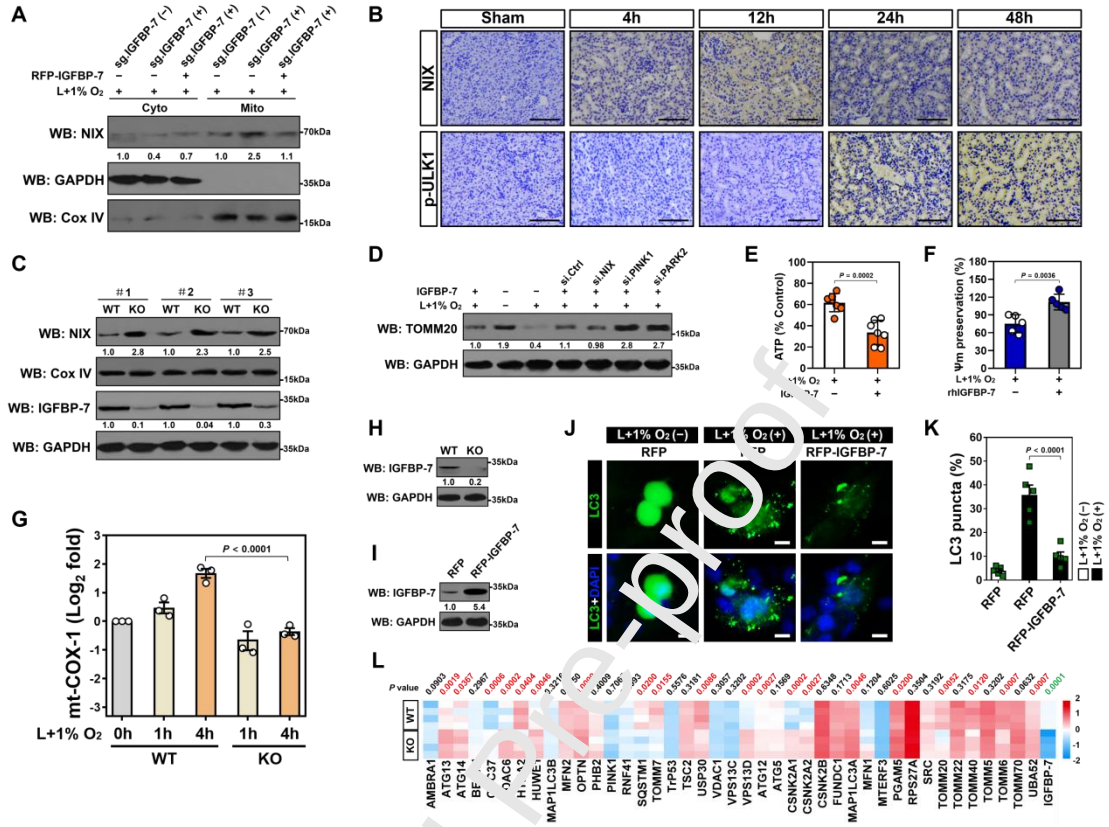

Fig. 6. IGFBP-7 rewires NIX-mediated mitophagy in response to ICTD. A: Western-blotting (WB) comparing levels of NIX protein in cytoplasmic and mitochondrial fraction of sgRNA (sg.IGFBP-7)-transduced RTECs with or without RFP-tagged IGFBP-7 re-expression in the presence of LPS plus hypoxia costimuli. B: Representative pictures of immunochemistry for NIX and p-ULK1_Ser555 staining in renal sections of mice after CLP challenge at the indicated timepoints. Scale bar = 100 μm. C: Western-blotting (WB) determining levels of NIX protein in mitochondrial fractions of kidney samples from *IGFBP-7*-WT or -KO mice with CLP. D: Western-blotting (WB) determining levels of TOMM20 protein in the LPS plus hypoxia-costimulated RTECs with IGFBP-7 treatment in the presence of siRNA targeting NIX (si.NIX), PINK1 (si.PINK1) or PARK2 (si.PARK2) transfection. E: Intracellular ATP levels of the LPS plus hypoxia-costimulated RTECs with or without IGFBP-7 treatment (n = 7 per group). F: Mitochondrial membrane potential (Ψm) of the LPS plus hypoxia-costimulated HK-2 cells with or without rhIGFBP-7 treatment (n = 5 per group). G: Cytosolic release of mitochondrial COX-1 (mt-COX-1) in *IGFBP-7*-WT or -KO RTECs with LPS plus hypoxia costimuli at the indicated timepoints (n = 3 per group). H: Western-blotting (WB) evaluating levels of IGFBP-7

protein in *IGFBP-7*-WT or -KO RTECs. I: Western-blotting (WB) evaluating levels of IGFBP-7 protein in RFP-tagged IGFBP-7-expressed RTECs. J and K: Immunofluorescence (J) and quantification (K) of LC3-positive puncta in RFP-tagged IGFBP-7-expressed RTECs with LPS plus hypoxia costimuli (n = 5 per group). L: Heat map of mitophagic gene expression in *IGFBP-7*-WT or -KO RTECs with LPS plus hypoxia costimuli. Data are expressed as mean ± s.d. (E, F, G, K). Two-sided Student's t test (E, F, L) and two-sided ANOVA with Bonferroni post hoc t test correction (G, K) was used to calculate the P value, respectively.

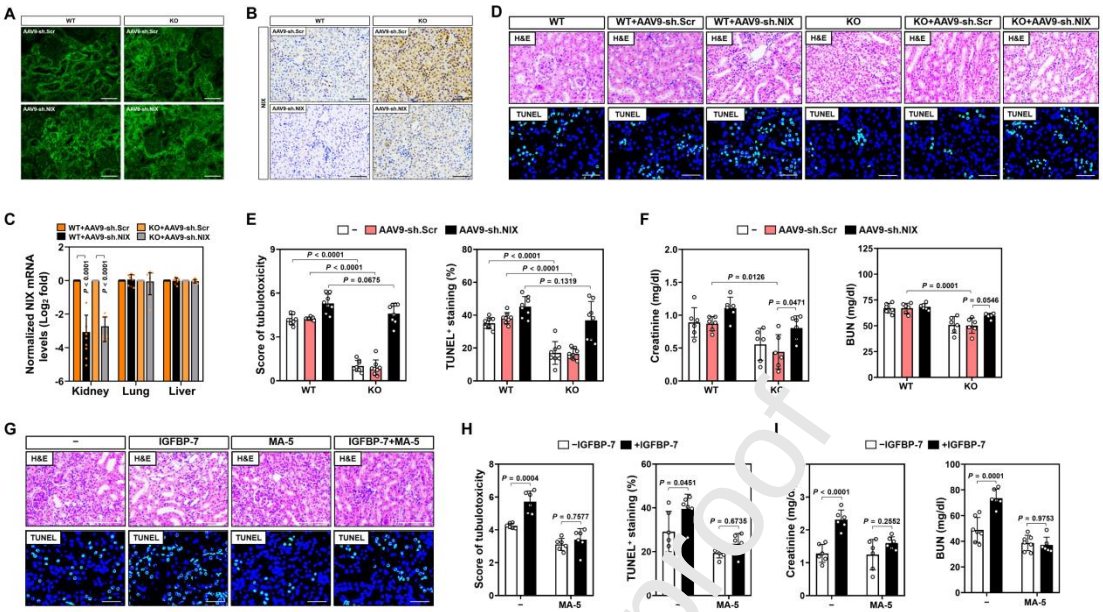

Fig. 7. Suppression of NIX-mediated mitophagy is instrumental for ICTD perpetuated by IGFBP-7 during septic AKI. A: Representative immunofluorescence images of GFP$^+$ staining in renal sections from *IGFBP-7*-WT or -KO mice receiving injection of adeno-associated viral 9 (AAV9) harboring scrambled (AAV9-sh.Scr) or NIX shRNA (AAV9-sh.NIX). Scale bar = 100 μm. B: Representative IHC images for NIX staining of renal sections from *IGFBP-7*-WT or -KO mice receiving injection of adeno-associated viral 9 (AAV9) harboring scrambled (AAV9-sh.Scr) or NIX shRNA (AAV9-sh.NIX). Scale bar = 100 μm. C: RT-qPCR analyses measuring NIX mRNA expression in whole kidney, lung and liver tissues from *IGFBP-7*-WT or -KO mice receiving injection of adeno-associated viral 9 (AAV9) harboring scrambled (AAV9-sh.Scr) or NIX shRNA (AAV9-sh.NIX) (n = 8 per group). D and E: Representative hematoxylin and eosin (H&E) and TUNEL images as well as quantification of renal sections from *IGFBP-7*-WT or -KO mice receiving injection of adeno-associated viral 9 (AAV9) harboring scrambled (AAV9-sh.Scr) or NIX shRNA (AAV9-sh.NIX) upon CLP challenge (n = 8 per group). Scale bar = 100 and 50 μm. F: Serum creatinine (Scr) and blood urea nitrogen (BUN) of *IGFBP-7*-WT or -KO mice receiving injection of adeno-associated viral 9 (AAV9) harboring scrambled (AAV9-sh.Scr) or NIX shRNA (AAV9-sh.NIX) upon CLP challenge (n = 6 per group). G and H: Representative hematoxylin and eosin (H&E) and TUNEL images as well as quantification of renal sections from CLP mice with or without injection of recombinant mouse IGFBP-7 and/or oral gavage of MA-5 (80 mg/kg) (n = 6 per group). Scale bar = 100 and 50 μm. I: Serum creatinine (Scr) and

blood urea nitrogen (BUN) of CLP mice with or without injection of recombinant mouse IGFBP-7 and/or oral gavage of MA-5 (80 mg/kg) (n = 6 per group). Data are expressed as mean ± s.d. (C, E, F, H, I). Two-sided ANOVA with Bonferroni post hoc t test correction (C, E, F, H, I) was used to calculate the P value.